ORIGINAL PAPER-EXPLORATION ENGINEERING

Determining the drilling mud window by integration of geostatistics, intelligent, and conditional programming models in an oilfield of SW Iran

Pooria Kianoush[1] · Ghodratollah Mohammadi[1] · Seyed Aliakbar Hosseini[2] · Nasser Keshavarz Faraj Khah[3] · Peyman Afzal[1]

Abstract

Accurate knowledge of pore and fracture pressures is essential for drilling wells safely with the desired mud weight (MW). Overpressure occurs when the pore pressure is higher than the normal hydrostatic pressure. There is a challenge regarding the pressure studies domain in an oilfield in SW Iran, where lack of geo-mechanical data limits exact mud window calculation. Also, the reservoir generally consists of carbonate rocks and contains no shale interbeds, so mechanical stratigraphy based on Gamma ray could not be applied. This study is to provide safe drilling considering MW to prevent the flow or loss in the vicinity of the new wells in the studied field. In this research, the formation pressures and mud window models are determined by combining geostatistical, intelligent, and conditional programming models and compared with real data. The conditional programming was also used to correct small out-of-range data. The highest correlation between the final effective pressure and velocity cube was observed in lower Fahliyan Formation with 0.86 and Ilam with 0.71.The modeled MW difference ranged between 2.5 and 30 PCF. Also, the maximum modeled MW is 150 PCF in the upper Fahliyan Formation. Heavy mud of more than 130 PCF is suggested for drilling the Khalij member and continues to the end of stratigraphy column. Best observed correlation comparing the drilled and modeled MW, especially achieved in the Fahliyan reservoir Formation with more than 100 PCF and the Ilam Formation with 80–100 PCF. Finally, 3D formation pressures are presented and recommended for further safe drillings.

Abbreviations

ANN	Artificial neural network
DDR	Daily drill report
DST	Drill stem test
FFBP-NN	Feed-forward back propagation neural network
IDW	Inverse distance weighted
LOT	Leak-off test
MDT	Modular dynamic tester
MW_{max}	Maximum mud weight
MW_{min}	Minimum mud weight
OB	Overburden pressure (psi)
OBG	Overburden stress gradient
PCA	Principal components analysis
PCF	Pounds per cubic foot
RFT	Repeat formation test
SGS	Sequential Gaussian simulation
SMWW	Safe mud weight window
VSP	Vertical seismic profiling

Nomenclatures

ρ (RHOB)	Density (gr/cm^3)
σ	Effective stress (psi)
P_{inj}^{min}	Minimum injection pressure
AI	Acoustic impedance [(m/s)*(g/cm^3)]

✉ Ghodratollah Mohammadi
  ghodratollah46@gmail.com; gh_mohammadi@azad.ac.ir

1 Department of Petroleum and Mining Engineering, South Tehran Branch, Islamic Azad University, Tehran, Iran

2 Department of Petroleum, Materials and Mining Engineering, Central Tehran Branch, Islamic Azad University, Tehran, Iran

3 Deputy Manager Geoscience Faculty, Research Institute of Petroleum Industry (RIPI), Tehran, Iran

k_0	The matrix stress or effective stress coefficient
p	Pore pressure (PSI),
P_p	Pore pressure gradient
V_p	Compressional velocity (m/s)
V_s	Shear velocity (m/s)
β	Constant
σ'_h	Effective minimum stress
σ_f	Fracture pressure
σ_h	Minimum stress
σ_t	Horizontal tectonic stress
σ_v	Vertical stress,
υ	Poisson's ratio

Introduction

Having correct understanding of the pore pressure of the formation is essential not only for the safe and economical drilling of wells but also for assessing exploration risk factors such as formation migration fluid and sediment integrity. Usually, before drilling, an initial estimate of the pore pressure from the surface seismic data is made by seismic velocities. Using seismic data is the only method to predict the pore pressure in the pre-drilling stage. It estimates the pore pressure based on the effect of wave velocity on pressure changes (Baouche et al. 2020; Sen and Ganguli 2019).

Seismic data, well logs, and drilling information are required information for determining the pore pressure gradient in a field. In case of a lack of necessary information in a part of the field after screening the available data and preparing the database, the necessary well logs are prepared using estimating models (Abdelaal et al. 2022; Haris et al. 2017; Jindal and Biswal 2016; Radwan et al. 2020; Radwan 2021). Sonic logs can be a good indicator of the internal pressure of the ground, i.e., increasing the sound passing time in the zones is a function of changing the porosity or increasing the pore pressure gradient, so that areas with abnormal pore pressure could be identified. Consequently, reduce drilling risk and related costs in these areas are achieved. In addition to pressure, other factors such as lithology also affect the speed of seismic waves; therefore, the use of available geological information and well logs can essentially prevent errors in estimating the pressure of the formation, especially in carbonate formations (Ganguli and Sen 2020; Ganguli et al. 2016, 2018; Kianoush et al. 2022; Radwan 2021).

According to the effective pressure information at wells (MDT/RFT/DST) and the overburden pressure cube created in the previous section, the effective stress at points of these wells can be calculated. For drilling exploration in the petroleum industry, fracture pressure is the pressure required to fracture the formation and to cause mud losses from a wellbore into the induced fractures. Fracture gradient is obtained by dividing the true vertical depth into the fracture pressure. The fracture gradient is the upper bound of the mud weight; therefore, the fracture gradient is an important parameter for mud weight design in both stages of drilling planning and operations. If the downhole mud weight is higher than the formation fracture gradient, then the wellbore will have tensile failures (i.e., the formation will be fractured), causing losses of drilling mud or even lost circulation (total losses of the mud). Therefore, fracture gradient prediction is directly related to drilling safety. The concept and calculation of fracture gradient probably first came from the minimum injection pressure proposed by Hubbert and Willis (1957). They assumed that the minimum injection pressure to hold open and extend a fracture is equal to the minimum stress. Later on, many empirical and theoretical equations and applications for fracture gradient prediction were presented (Aadnoy and Larsen 1989; Althaus 1975; Anderson et al. 1973; Breckels and van Eekelen 1982; Constant and Bourgoyne 1988; Daines 1982; Eaton 1969; Fredrich et al. 2007; Haimson and Fairhurst 1967; Keaney et al. 2010; Matthews and Kelly 1967; Oriji and Ogbonna 2012; Pilkington 1978; Saadatnia et al. 2022; Wessling et al. 2009; Zhang 2011; Zhang et al. 2022).

In this study, some commonly used methods are described in the following sections. It is known that there is a lower limit of mud weight (MW) below which compressive failure occurs and an upper limit beyond which tensile failure occurs. The range between the lower and the upper limit is defined as the MW window (Abdideh and Fathabadi 2013; Aslannezhad et al. 2016; Liguo et al. 2020; Radwan 2020; Yin et al. 2022). The intervals of tensile and shear rock failure are required to determine the safe MW window and the best drilling trajectory. The pressure of the drilling mud will cause a tensile failure in the wellbore, and drilling mud will be lost in the formation of the MW applied higher than the safe mud window. Shear failure or breakout will occur while this weight is applied lower than the safe mud window (Baouche et al. 2022; Darvishpour et al. 2019; Le and Rasouli 2012; Zhang 2013, 2019; Zhang et al. 2022; Zoback et al. 2003). If geomechanical parameters are unavailable, the equivalent MW is calculated using a confidence interval called a safety margin of about ± 200 pounds per square inch (PSI).

In computer science, conditionals are programming language commands for handling decisions. Specifically, conditionals perform different computations or actions depending on whether a programmer-defined Boolean condition evaluates to true or false. The decision is always achieved in control flow by selectively altering the control flow based on some condition (Vessey and Weber 1984). Conditional statements allow us to change how our program behaves based on the input it receives, the contents of variables, or

other factors. The most common and useful conditional for us to use in bash is the "if" statement (Andress and Linn 2016). The "if-then-else" construct is common across many programming languages. Here, using Petrel (2016) software, conditional programming has been widely used, such as combining logs in different parts of a field, adding and subtracting cubes, and extracting out-of-range data from generated cubes by undefined codding.

Sequential Gaussian simulation (SGS) is typical in geostatistical simulations, and in many simulators, it has responded to porosity, permeability, and other regional variables. In this method, the simulated value at each point is obtained using the probability distribution function calculated from the raw data and the previous simulation data in the nearest neighbors of the desired point. The first principle in all Gaussian methods is the normality of the raw data; otherwise, they must become the standard (Hosseini et al. 2019; Kelkar and Perez 2002; Lantuéjoul 2001; Zhang et al. 2017).

In the co-kriging method, the evaluation is performed using the correlation between the desired regional variable and the auxiliary variable in places with a shortage of samples. If the correlation between the two variables is greater than 0.5, the estimation error is significantly reduced by this method (Armstrong et al. 2011; Bohling 2007).

Intelligent methods such as Artificial Neural Networks (ANN) can simulate the ability to receive signals and appropriate responses from the biological neural network and are used in countless fields, including the oil industry are the methods with low cost and high accuracy. ANN is widely used in safe mud windows estimation. After designing and training neural networks and estimating logs or cubes in each zone, the generalization of the networks and the convergence between the actual and estimated values in each zone should be investigated and analyzed. In recent years, ANN has been used to predict the formation gradient and compare their performance. The study showed that ANN provides a sufficient approximation of the fracture gradient as a function of depth, overburden pressure gradient, and Poisson's ratio, but the values of the fracture gradient (Sadiq and Nashawi 2000). Hu et al. (2013) proposed a new feed-forward back propagation artificial neural network (FFBP-ANN) structure to determine pore pressure. It could partially remove the input data from the non-shale formation to show the lithological effect (Hu et al. 2013; Sadiq and Nashawi 2000). Khatibi and Aghajanpour (2020) introduced ANN approaches for shear sonic log prediction, comparing with the empirical Greenberg–Castagna method. Gowida et al. (2022) introduced a new approach to develop a new ANN data-driven model to estimate the safe mud weight range in no time and without additional cost. Beheshtian et al. (2022) developed a novel ANN method to predict Safe mud window from ten well-log input combined with machine learning algorithm hybridized with optimizers.

In the cited previous research, there were all the required data for mud window calculations, and it mainly focused on predicting mud windows in limited reservoir formations. Since this study required the mud window in multi-reservoir formations, we faced some limitations. Deficiency of geomechanical properties of core samples and leak-off test data to estimate and validate breakouts, breakdown, and formation fracture gradients were the first constrain. Furthermore, the mechanical stratigraphy method could not be involved since the dominant lithology of the target reservoir formation is Limestone and does not include shale content. However, gamma-ray logs were available and used for ANN layers.

Considering the vast areal content of the Azadegan oil field (740 Km^2) and generated acoustic impedance cube obtained from seismic inversion (AI), the combination of geostatistical methods of sequential Gaussian simulation (SGS) and co-kriging is used for the first time to construct the final models of the formation pressure cube in the entire studied area. Also, utilizing conditional programming (e.g., sequential and nested conditional expressions) to combine logs and cubes in a single model while removing out-of-range values is a novel approach in this study.

Another innovation in this article was implemented to compensate for the data shortage and extent of the research area. First, validating the minimum and maximum mud weight cubes based on the graphic well logs derived from daily drilling reports and inspecting the mud weight alteration leading to losses and flows in each formation and depth have been examined. Secondly, out-of-range values are revised separately by combinatorial conditional programming. Consequently, for data validation, without employing the core and leak-off test data, the upper and lower limits of the mud window have been obtained as an accurate and reliable source (Appendix A).

Geological setting

Geological model based on seismic interpretation

The Azadegan oilfield is located in the transition zone between the Arabian plate and the Zagros basin (Fig. 1). The Zagros orogeny has changed the shape and fracture of the subsurface layers due to the presence of shale and marl in the Cenozoic formations and the reduction in tectonic stress which have a sealing role in restraining the migration and vertical loss of oil (Du et al. 2016; Mehrkhani et al. 2019). The seismic profile across Azadegan high shows a steep fault system in the Jurassic and underlying sedimentary rocks (Abdollahie Fard et al. 2006; Morgan 1999).

Figure 2a shows a cross section that is horizontally flattened at the top Bangestan Group level. Other horizons are correspondingly shifted in Fig. 2b. The flattened cross

Fig. 1 Structural map of the Abadan Plain. Major anticlines appear as elongated domes. The location of studied area and seismic profiles are outlined with red polygon (Abdollahie Fard et al. 2006)
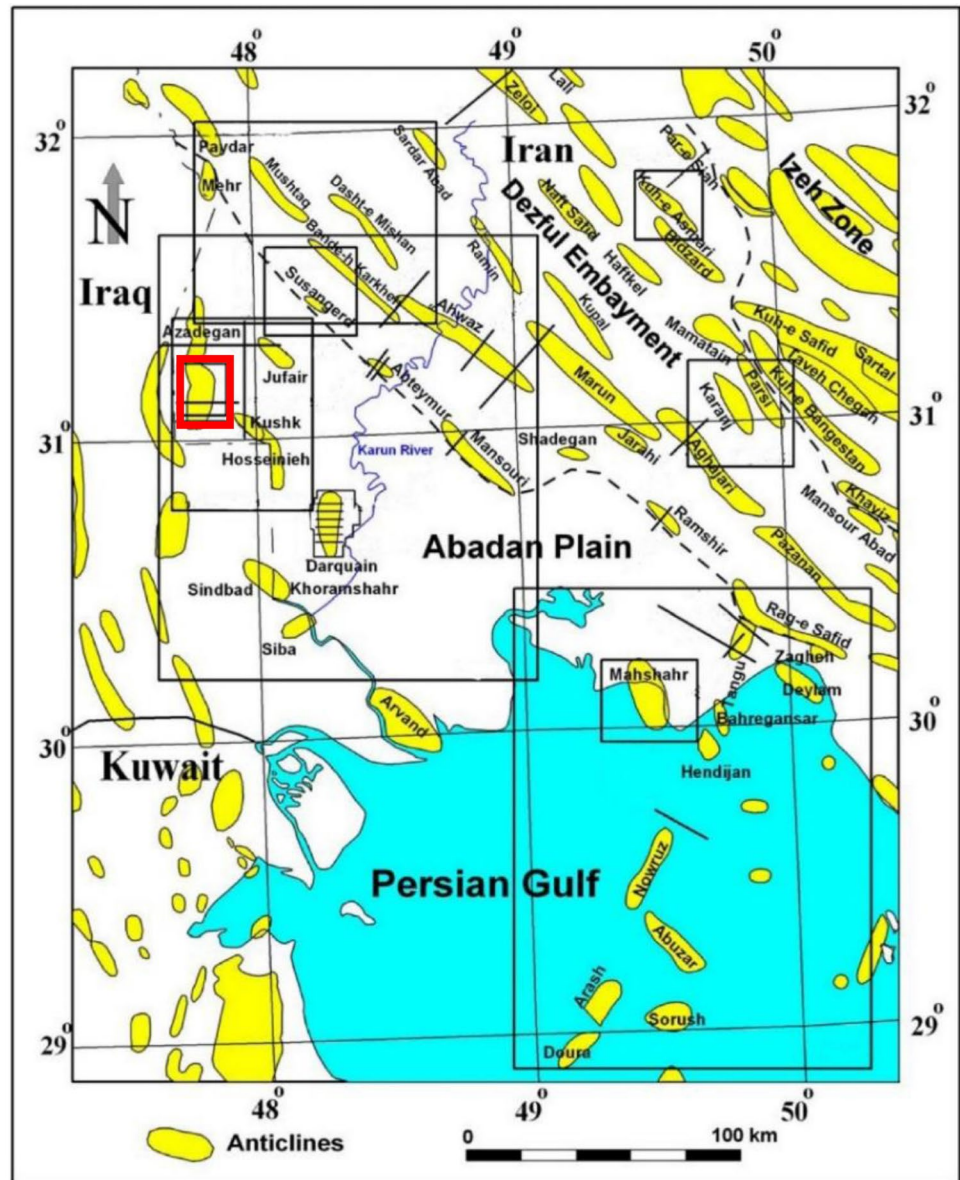
section shows that the uplifting of the Burgan-Azadegan High was continued in Late Cretaceous and Tertiary (Abdollahie Fard and Hassanzadeh-Azar 2002). The Azadegan structure is presented as a nearly symmetric gentle relief with 3° and 1° eastern and western flanks, respectively. Figure 2.b shows thinning of the Mid Cretaceous Bangestan Group and the Late Cretaceous Gurpi Formation in the crest of the Azadegan Anticline (Abdollahie Fard et al. 2006; Morgan 1999).

Mechanical stratigraphy can provide valuable knowledge for evaluating and predicting the distribution of structural fractures and in situ stress by the core analysis. In terms of geological interpretation, the commonly used sequence stratigraphy analysis includes a lithofacies analysis. The most application of sequence stratigraphy is in shale formations

using gamma Ray log because it measures naturally occurring gamma radiation from shales (Lee et al. 2018; Liu et al. 2022; Woo et al. 2022).

Study area includes the South Azadegan Field, which out of 42 available wells, 23 wells have the most selected information. 17 wells located in the central, western, and southern parts have effective pressure test (DST) data and MDT logs in the Ilam to Fahliyan reservoir Formation intervals.

Construction of the structural geological model

The studied field formations are modeled based on the interpretation of time-domain seismic horizons data and correlated with drilling geological information. Depth-domain seismic horizons have been constructed
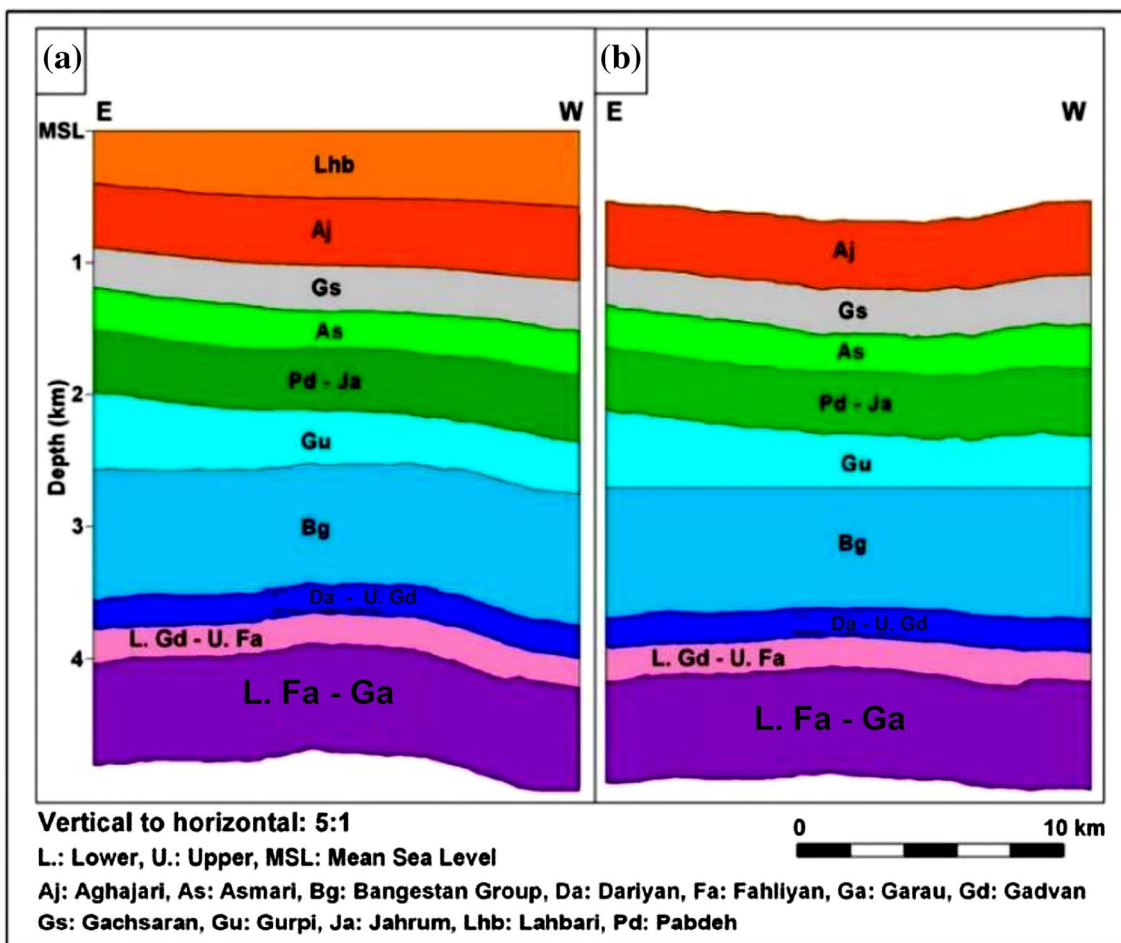
Fig. 2 a A structural cross section of the Azadegan Anticline in E-W direction. **b** The structural cross section is flattened at the top Bangestan Group (Abdollahie Fard et al. 2006)

as separate surfaces from the Aghajari to the Gotnia Formations. Due to the lack of complex fault systems in the area, the geological model has been built with a simple network (Fig. 3 and Table 1).

Methodology

Compressional wave velocity modeling

Compressional velocity cube as the initial data has been modeled using geostatistical approaches such as SGS and co-kriging with the same coordinates and inverse distance weighted (IDW) method by determining the relationships between inverted acoustic impedance cube from seismic data, as a trend and scaled-up sonic logs in 23 available wells (Fig. 4).

Overburden pressure cube

Overburden pressure cube is the pressure caused by the overburden weight of the rock matrix and the fluids in the pore space of the overlying rock column. It is also known as geostatic pressure. For estimating the pore pressure with velocity data, the relationship between effective stress and velocity in sediments under normal pressure has been proposed by Bowers (Eq. (1)):

$$V = V_0 + A\sigma^B \tag{1}$$

where V_0 is the velocity of unconsolidated fluid-saturated sediments. A and B describe the variation in velocity with increasing effective stress (σ) and can be derived from offset well data (Bowers 1995, 2002). The overburden pressure cube is calculated by integrating the average density value (from the surface to the desired depth). In Gardner's method,
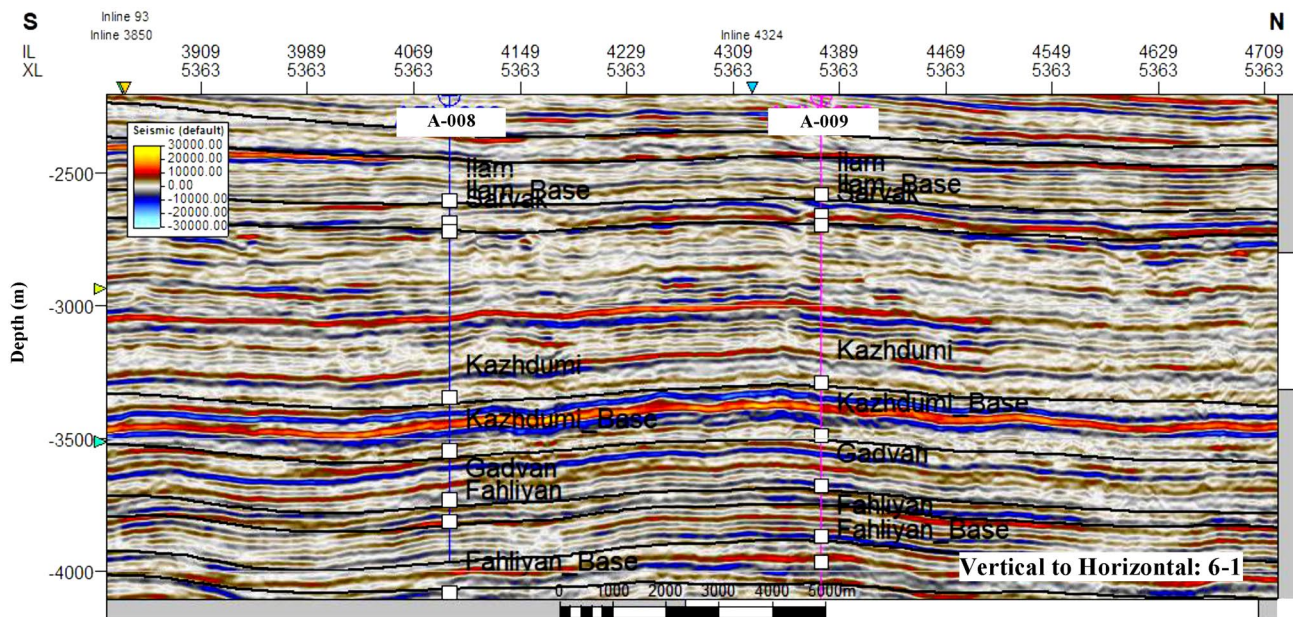
Fig. 3 Sample of seismic data section with formation top, depth domain seismic sections, and location of exploratory wells in South Azadegan Field (Kianoush et al. 2022)

Table 1 Division of South Azadegan Field based on the average cubic thickness of geological layers (using Petrel 2016 software)

Row	Formation	Formation top (m)	Formation base (m)	Average thickness (m)	Dominant lithology	Number of data cubes
1	Aghajari	0	1272.3	1272.3	Marl and sandstone	14,090
2	Gachsaran	1272.3	1630.65	358.35	Anhydrite and claystone	7,571
3	Asmari	1630.65	2368.25	737.6	Sandstone and limestone	17,579
4	Gurpi	2368.25	2590.05	221.8	Limestone	26,650
5	Tarbur (Member)	2590.05	2757.85	167.8	Limestone and marl	93,179
6	Ilam and Laffan	2757.85	2866.05	108.2	Limestone and claystone	64,678
7	Sarvak	2866.05	3506.9	640.85	Limestone	382,420
8	Kazhdumi	3506.9	3733.95	227.05	shale, limestone and sandstone	150,607
9	Dariyan	3733.95	3896	162.05	Limestone and marl	134,788
10	Gadvan	3896	3966.55	70.55	Marl, shale and limestone	85,320
11	Khalij (member)	3966.55	4071	104.45	Sandstone and limestone	139,131
12	Upper Fahliyan	4071	4228.05	157.05	Limestone	190,818
13	Lower Fahliyan	4228.05	4589.1	361.05	Limestone	199,299
14	Garau	4589.1	4783	193.9	Limestone and claystone	75,612
15	Gotnia	4783	4931	148	Anhydrite and limestone	45,221
16	Najmeh	4931	4959	28	Anhydrite and limestone	6,678
17	Sargelu	4959	5068	109	Limestone and shale	17,858
18	Alan	5068	5107	39	Anhydrite and limestone	3,900
19	Muss	5107	5199	92	Limestone	7,089
20	Neyriz	5199	5590	391	Limestone and anhydrite	7,873

first, the logarithmic diagram of the completed cubes of the density logs is plotted relative to the compression velocity logs (Gardner et al. 1974), and the logarithmic relation obtained becomes the exponential Eq. (2).

$$\rho = aV_P^b \qquad (2)$$

Logarithmic relation of density cube graphs to compression velocity of South Azadegan Field generated from
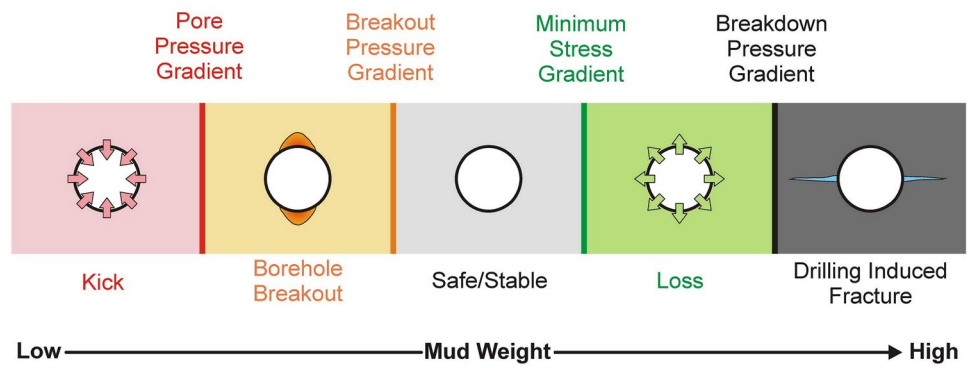
the checkshots data and vertical seismic profiling (VSP) is shown in Fig. 5.

In another method, the mean density is obtained through the Amoco experimental relation based on depth in meters. (Eq. (3)).

$$\rho_{avg} = \frac{\left(16.3 + \frac{3.281 \times \text{Depth}}{3125}\right)^{0.6}}{8.354} \quad (3)$$

Due to the high correlation coefficient between the Gardner relation and the Amoco relation of 92.4%, the use of the density cube obtained from the Gardner relation coefficients is approved due to its higher accuracy.

To calculate the overburden pressure, given that the product of density (grams per cubic centimeter) in gravity acceleration (9.81 m per second squared) at depth (meters) is obtained in kilopascals, to calculate the pressure in PSI requires a conversion factor of 145.038/1000; thus, the relationship is as follows (Eq. (4)):

$$P_{O.B} = \frac{9.81 \times \rho_{avg} \times \text{Depth} \times 145.038}{1000} \quad (4)$$

Effective pressure cube

The effective pressure cube (also known as differential pressure) governs the compaction process in sedimentary rocks. Geopressuring implies that the rock has low effective stress and a higher porosity than would be expected when the rock was normally compacted; it results in a lower rock velocity (Dutta et al. 2021). Pressure test data of the studied field generally start from Sarvak and continue to Gotnia Formation, but data in the upper formations are minimal (Fig. 6). By considering obtained data from these 23 wells, the initial modeling of the effective pressure was done using three methods: Bowers using velocity cube (co-kriged with AI), SGS (co-kriging with Vp), and IDW method.
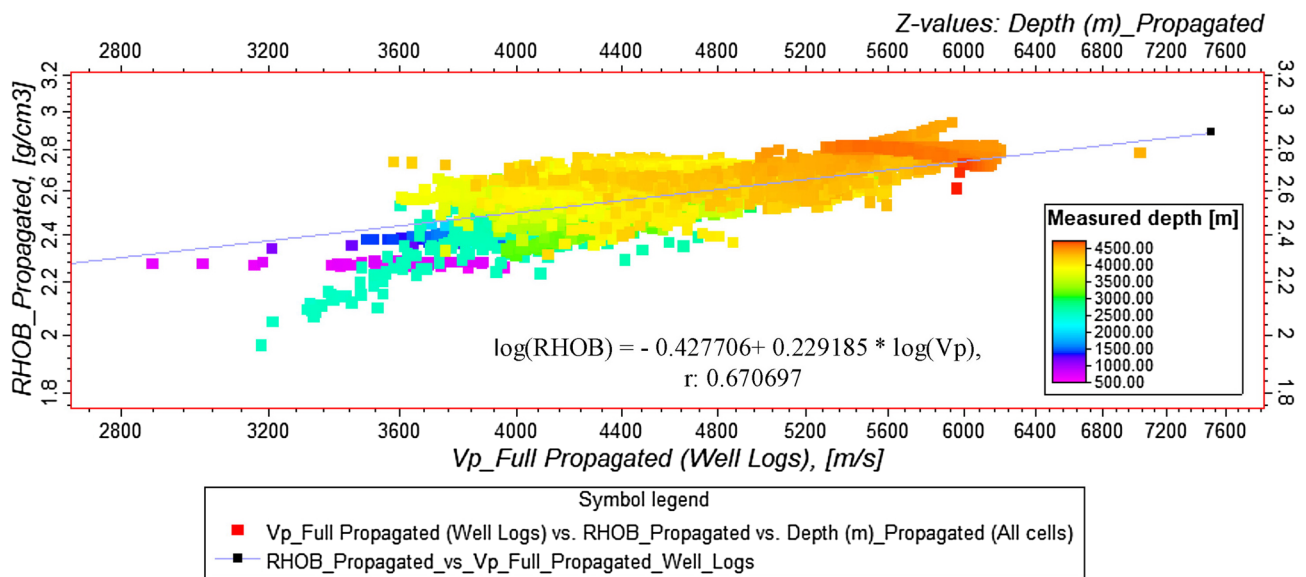

Fig. 5 Logarithmic relation of density cube graphs to compression velocity of South Azadegan Field
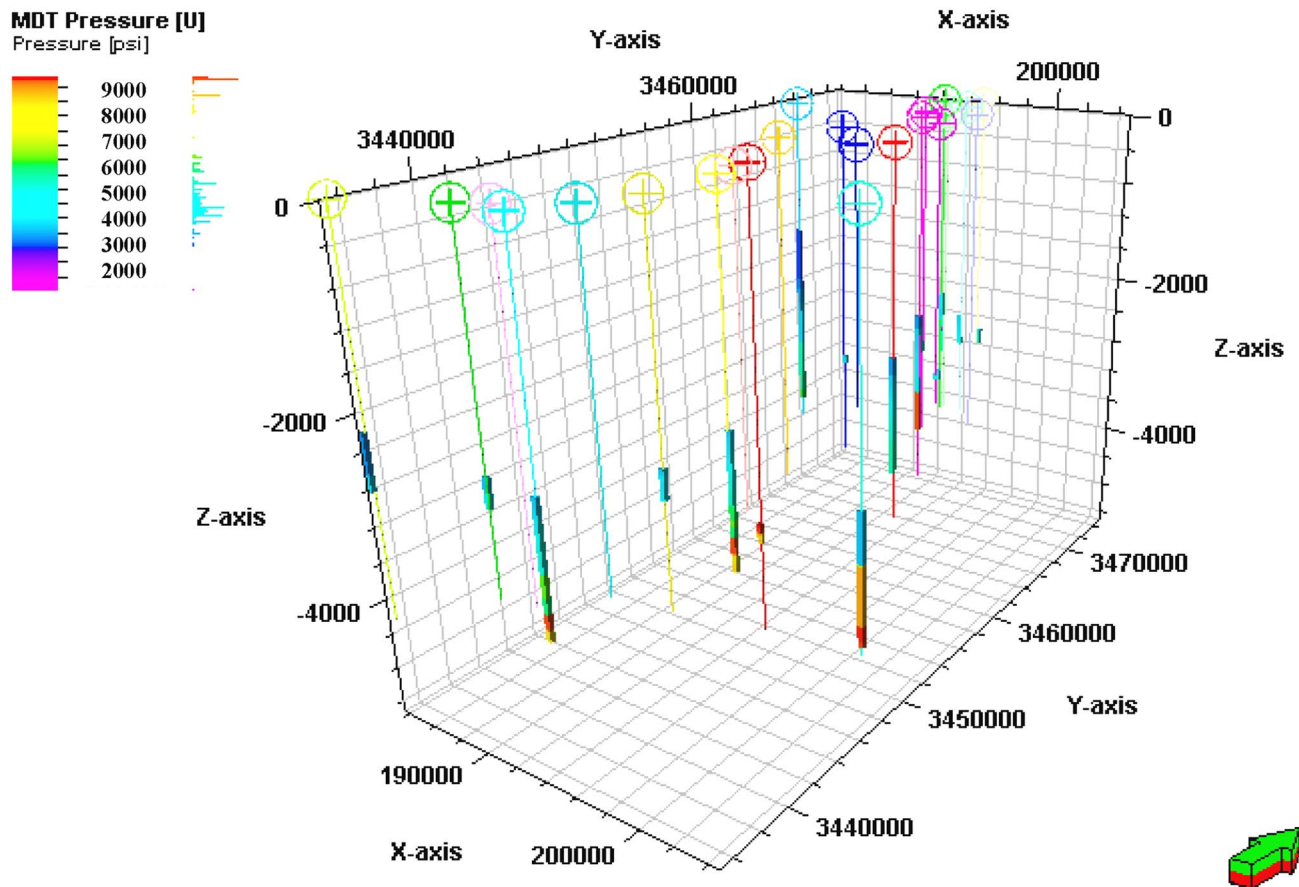
Fig. 6 Initial scale-up effective pressure model resulting from MDT well logging data and DST pressure tests

Bowers method

In this method, the exponential relationship of the initial MDT effective pressure data with the final velocity cube (made by the SGS method and co-kriged with AI) for different formations is analyzed separately (Fig. 7 and Table 2). Then, the effective pressure log for each of the wells was calculated and produced separately using conditional programming in Petrel (2016) software. An example is presented in Eq. (5).

Sequential Gaussian simulation (SGS) and co-kriging method

In this method, the initial scaled-up model of MDT pressure is made from Asmari to lower Fahliyan Formations using the SGS method combined with co-kriging (with Vp and AI cubes). The next step was completed using the

$$
\begin{aligned}
&\text{Effective\_Pressure\_Bowers} = \\
&\quad \text{If(DEPT} >= 1773 \text{ and DEPT} < 2604.34, \text{ Pow(Vp\_Full\_SGS\_AI}/1805.801, 1/0.102684), \\
&\quad \text{If(DEPT} >= 2604.34 \text{ and DEPT} < 2695, \text{ Pow(Vp\_Full\_SGS\_AI}/68.049, 1/0.488238), \\
&\quad \text{If(DEPT} >= 2695 \text{ and DEPT} < 3332, \text{ Pow(Vp\_Full\_SGS\_AI}/3139.93, 1/0.0472037), \\
&\quad \text{If(DEPT} >= 3332 \text{ and DEPT} < 3536, \text{ Pow(Vp\_Full\_SGS\_AI}/6355.211, 1/-0.030526), \\
&\quad \text{If(DEPT} >= 3536 \text{ and DEPT} < 3723.64, \text{ Pow(Vp\_Full\_SGS\_AI}/6136.489, 1/(-0.025068)), \\
&\quad \text{If(DEPT} >= 3723.64 \text{ and DEPT} < 3780.9, \text{ Pow(Vp\_Full\_SGS\_AI}/5415.144, 1/(-0.036573)), \\
&\quad \text{If(DEPT} >= 3780.9 \text{ and DEPT} < 3920.92, \text{ Pow(Vp\_Full\_SGS\_AI}/3929.1625, 1/(-0.00881239)), \\
&\quad \text{If(DEPT} >= 3920.92 \text{ and DEPT} < 4090, \text{ Pow(Vp\_Full\_SGS\_AI}/3770.075, 1/0.0171153), \\
&\quad \text{If(DEPT} >= 4090 \text{ and DEPT} < 4334, \text{ Pow(Vp\_Full\_SGS\_AI}/39.7502, 1/0.537257), \text{ U)))))))))}
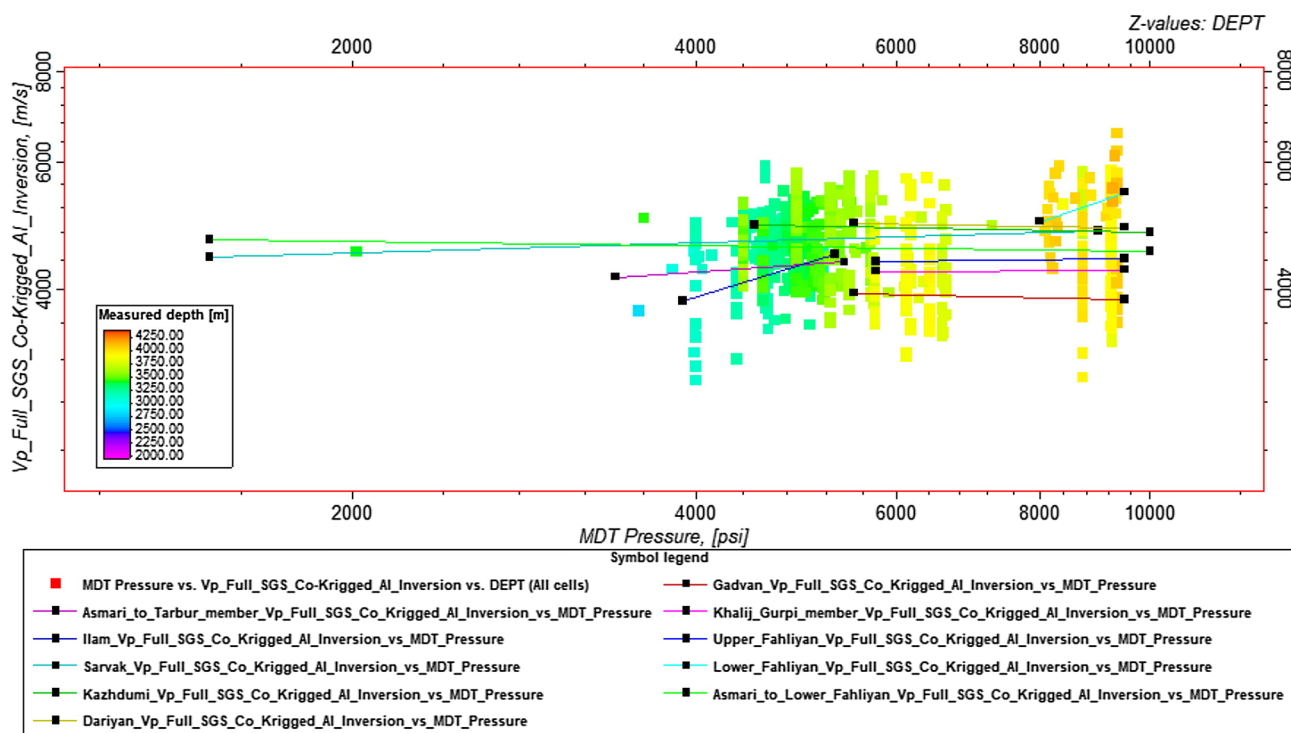\end{aligned}
\tag{5}
$$

Fig. 7 Calculation of Bowers coefficients based on the MDT and DST effective pressure against the final Compressional velocity cube (VP_Full_SGS and co-kriging with AI_Inversion)

neural network of the above model. Furthermore, it was validated after estimating the pore pressure cube with the primary data.

Inverse distance square weighted (IDW) method

In this method, using the initial scaled-up MDT model, the initial cube of effective pressure is made by the IDW method from the Asmari to the lower Fahliyan Formations. Furthermore, like the previous two models, the above model is completed using the ANN in the next step.

Complementary effective pressure model using neural network

In this step, information layers by the principal component analysis (PCA) were chosen for full propagation of primary effective pressure cubes by the feed-forward back propagation (FFBP-NN) method to determine the highest correlation coefficient with initial MDT data. The correlation between 0.2 and 0.3 (green values) is suitable for generating an ANN layer, and values below 0.2 (blue values) have a low correlation (Table 3).

Five information layers were used to modify the model, including gamma, Vp, AI, density, and overburden pressure. Among the selected layers of gamma cubes, Vp and AI have

a correlation coefficient in the acceptable range, and density and overburden pressure have also been selected due to their direct impact on other formation pressures (Table 4). Based on the general comparison of the histograms, the most similar frequency distribution in completed effective pressures is related to the SGS method in Ilam Formation with the range of 3500–4550 PSI (Fig. 8).

Also, based on the comparison of the three methods, the FFBP-ANN model based on the initial SGS with 30 iterations has the training error values of 1083.53, test error of 1083.64, and relative error of 0.536. It has the lowest error values compared to the other two methods. Therefore, the effective pressure cube modeled with the integration of SGS, co-kriged with V_P and AI, and the FFBP-NN methods is more accurate than the other two methods.

Pore pressure cube

The well test data among the 17 selected wells are discontinuous. Well test pressure log (MDT) must be estimated for the wells in the side sections to calculate the pore pressure gradient in the whole field. For this purpose, pore pressure cube is the pressure acting on the fluids in the pore space of a formation. It is equal to the hydrostatic pressure plus the over-(or under) pressure. Based on the Terzaghi et al. (1996) relationship (Eq. (6)), each of the

Table 2 Calculation of Bowers coefficients based on the MDT and DST effective pressure against the completed velocity log (VP$_{Full}$_SGS_co-kriged_AI)

Row	Formation	Logarithmic relation (P$_{eff}$ ~ Vp·$_{SGS.AI}$)	Correlation coefficient (r)	A & b coefficients	Bowers relation (Vp=a.Peff^b)	Effective pressure (P$_{eff}$)
1	Asmari to Gurpi	Log(Y)=0.102684* log(X)+3.25667	0.174	a=1805.801, b=0.102684	Vp=1805.801*Peff0.102684	P$_{eff}$=(Vp.SGS. AI/1805.801) (1/0.102684)
2	Ilam	log(Y)=0.488238* log(X)+1.83282	0.252	a=68.049, b=0.488238	Vp=68.049*Peff0.488238	P$_{eff}$=(Vp.SGS. AI/68.049) (1/0.488238)
3	Sarvak	log(Y)=0.0472037* log(X)+3.49692	0.060	a=3139.93, b=0.0472037	Vp=3139.93*Peff0.0472037	P$_{eff}$=(Vp.SGS. AI/3139.93) (1/0.0472037)
4	Kazhdumi	log(Y)=−0.0305226* log(X)+3.80313	−0.046	a=6355.211, b=−0.0305226	Vp=6355.211*Peff-0.0305226	P$_{eff}$=(Vp.SGS. AI/6355.211)(1/- 0.030522)
5	Dariyan	log(Y)=−0.0250681* log(X)+3.78792	−0.335	a=6136.489, b=−0.025068	Vp=6136.489*Peff-0.025068	P$_{eff}$=(Vp.SGS. AI/6136.489)(1/- 0.025068)
6	Gadvan	log(Y)=−0.036573* log(X)+3.73361	−0.057	a=5415.144, b=−0.036573	Vp=5415.144*Peff-0.036573	P$_{eff}$=(Vp.SGS. AI/5415.144)(1/- 0.036573)
7	Khalij member	log(Y)=0.00881239* log(X)+3.5943	0.016	a=3929.162586, b=0.0088123	Vp=3929.1625*Peff 0.0088	P$_{eff}$=(Vp.SGS. AI/3929.162) (1/0.0088123)
8	U. Fahliyan	log(Y)=0.0171153* log(X)+3.57635	0.018	a=3770.075, b=0.017115	Vp=3770.075*Peff0.0171153	P$_{eff}$=(Vp.SGS. AI/3770.075) (1/0.0171153)
9	L. Fahliyan	log(Y)=0.537257* log(X)+1.59934	0.384	a=39.7502, b=0.537257	Vp=39.7502*Peff0.537257	P$_{eff}$=(Vp.SGS. AI/39.7502) (1/0.537257)

P_{eff} Effective Pressure, $Vp._{SGS.AI}$ Compressional Velocity using Sequential Gaussian Simulation (SGS) combined Co-kriging with Acoustic Impedance (AI)

Table 3 Linear correlation of the principal component analysis (PCA) of the final effective pressure neural network model obtained from the initial models

Linear Correlation	GR Propagated Moving Average	AI_m_Seismic_Inversion_Final_Propagated	Vp_Full Propagated (Well Logs)	RHOB Propagated	Overburden_Pressure_Real_Psi	MDT Effective Pressure Propagaed with Moving Average
GR Propagated Moving Average	1.0000	0.1836	0.3527	0.1827	0.2067	0.3258
AI_m_Seismic_Inversion_Final_Propagated	0.1836	1.0000	0.7146	0.5257	0.5264	0.3497
Vp_Full Propagated (Well Logs)	0.3527	0.7146	1.0000	0.6485	0.5425	0.3099
RHOB_Propagated	0.1827	0.5257	0.6485	1.0000	0.7655	0.6975
Overburden_Pressure_Real_Psi	0.2067	0.5264	0.5425	0.7655	1.0000	0.8951
Total	**0.6656**	**0.7341**	**0.8600**	**0.8440**	**0.7907**	**0.9275**

GR Gamma Ray, *RHOB* Density, *Vp* Compressional Velocity, *MDT* Modular Dynamic Tester

completed effective pressure cubes is deducted from the overburden pressure cube. Furthermore, after correlating the pore pressure cubes made with the initial MDT/DST pressure data for different formations (Table 5), the SGS model has the highest correlation coefficient, which is confirmed. Thus, data obtained from this method are considered to calculate the final pore pressure gradient.

$$P_{Pore} = P_{O.B} - P_{eff} \qquad (6)$$

Table 4 Correlation coefficients (r) of the principal components analysis (PCA) of the final neural network model of effective pressure obtained from the initial models by Bowers, SGS, and IDW methods

Correlation coefficients of bowers, SGS & IDW method	PC0	PC1	PC2	PC3	PC4
GR Cube	0.0677	0.9523	0.2282	0.1475	0.1214
Seismic acoustic impedance Inversion (AI) cube	−0.8173	−0.2393	0.5137	−0.0411	−0.0955
Vp (Well Logs) cube	−0.8681	−0.3534	−0.0891	0.2105	0.2630
RHOB Density Cube	−0.8660	0.3069	−0.2376	0.2135	−0.2320
Overburden Pressure cube	−0.8307	0.3625	−0.1460	−0.3901	0.0709
Eigenvalue	**2.8662**	**1.3146**	**0.4017**	**0.2656**	**0.1519**
Contribution (%)	**57.32**	**26.29**	**8.03**	**5.31**	**3.04**
Cumulative Contribution (%)	**57.32**	**83.62**	**91.65**	**96.96**	**100.00**

GR Gamma Ray, *RHOB* Density, *Vp* Compressional Velocity, *MDT* Modular Dynamic Tester
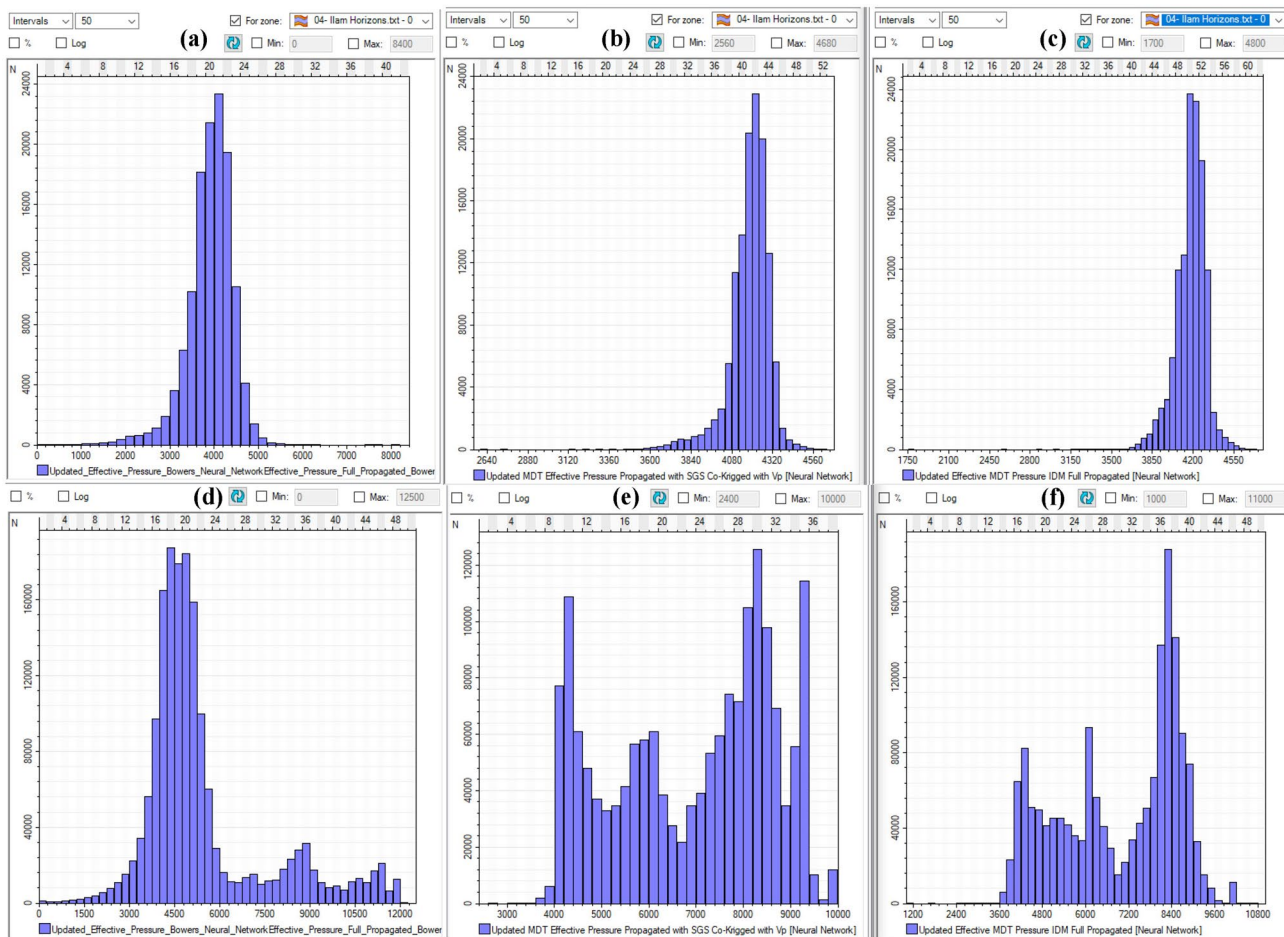
Fig. 8 Histogram comparison of the modeled effective pressure data of Ilam Formation by methods **a** Bowers (left column), **b** SGS (middle column) and **c** IDW (right column), and **d–f** in the whole study field (according to the top row)

Data validation of final pore pressure model

The effective pressure (PSI) in each formation of the final cube is compared with the Vp cube for the same formations. Finally, the Bowers relation coefficients are recalculated (Fig. 9).

Accordingly, the highest correlation coefficient between the final effective pressure cube and the velocity cube is related to the lower Fahliyan Formation with 0.86 and Ilam

Table 5 Correlation coefficients of formation pore pressure cubes of studied field using neural network based on Bowers, SGS, and IDW models with primary MDT data

Formation	Correlation coefficient of pore pressure and primary MDT data		
	Bowers method	SGS method	IDW method
Tarbur (member of Gurpi)	0.93	0.73	0.57
Ilam	0.12	0.47	0.34
Sarvak	0.24	0.48	0.48
Kazhdumi	0.07	0.14	0.09
Dariyan	0.19	0.27	− 0.1
Gadvan	0.36	0.14	− 0.4
Khalij (member of Gadvan)	0.27	0.19	− 0.49
Upper Fahliyan	0.21	0.22	− 0.06
Lower Fahliyan	− 0.25	− 0.57	0.1
Total MDT Data	0.58	0.57	0.44

with 0.71, which indicates the high accuracy of the modeled data with the original data (Table 6).

Anisotropic spatial variation in final pore pressure cube

For evaluating anisotropy variations in the final pore pressure cube, experimental variograms with the Gaussian method were created in three directions: vertical, major horizontal azimuth of zero degrees, and minor azimuth of 270 degrees. In the vertical variogram, the sill is 0.937, and

in major and minor is 1. The anisotropy range for vertical variogram is 68 m and for major and minor directions is 11850 m (Tables 7, and 8, and Fig. 10).

Fracture pressure cube

Fracture pressure is the pressure required to fracture the formation and to cause mud losses from a wellbore into the induced fractures. Some current methods for fracture pressure prediction are as follows:

Hubbert and Willis' method

The concept and calculation of fracture gradient probably first came from the minimum injection pressure proposed by Hubbert and Willis (1957). They assumed that the minimum injection pressure to hold open and extend a fracture is equal to the minimum stress (Eq. (7)):

$$P_{inj}^{min} = \sigma\prime_h + p = \sigma_h \qquad (7)$$

where P_{inj}^{min} is the minimum injection pressure; σ'_h is the effective minimum stress; σ_h is the minimum stress; and p is the pore pressure.

Matthews and Kelly's method

Matthews and Kelly (1967) introduced a variable of the "matrix stress coefficient (k_1)," equivalent to effective stress
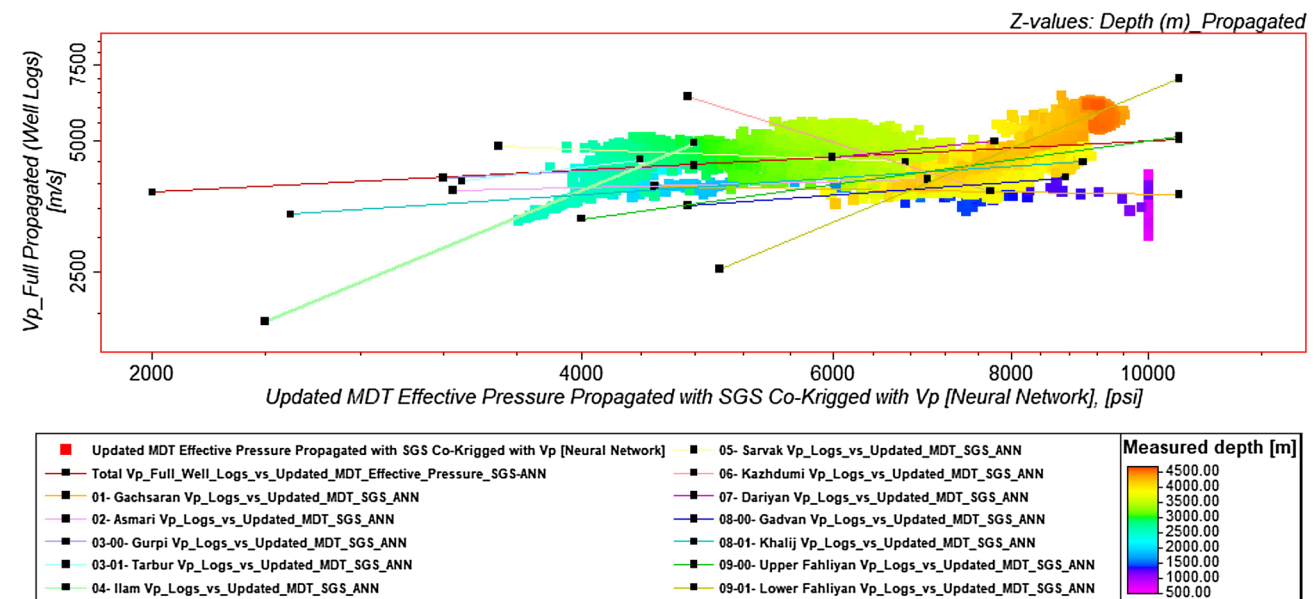

Fig. 9 Correlation coefficients of the final effective pressure model with the velocity cube model (update of the Bowers relation coefficients) in the whole field

Table 6 Parameters and correlation coefficients (r) of final Effective Pressure and Compressional Velocity cubes for updated Bowers relations in different formations of the studied field

Formation	$V = a P_{eff}{}^b$	r
Gachsaran	$A = 6112.23, B = -0.052$	-0.17
Asmari	$A = 2006.3, B = 0.077$	0.32
Gurpi	$A = 1055.9, B = 0.1682$	0.45
Tarbur (Member)	$A = 151.68, B = 0.405$	0.26
Ilam	$A = 0.043, B = 1.374$	**0.71**
Sarvak	$A = 13,720, B = -0.127$	-0.27
Kazhdumi	$A = 33,078.3, B = -1.025$	-0.65
Dariyan	$A = 290.35, B = 0.318$	0.44
Gadvan	$A = 439.7, B = 0.247$	0.25
Khalij (member)	$A = 613.49, B = 0.218$	0.19
Upper Fahliyan	$A = 77.5, B = 0.453$	0.55
Lower Fahliyan	$A = 0.023, B = 1.363$	**0.86**
Total field	$A = 1042.46, B = 0.1705$	0.38

P_{eff} Effective Pressure, r correlation coefficients

coefficient, for calculating the fracture gradient of sedimentary formations (Eq. (8)):

$$FG = k_0(OBG - P_p) + P_p \tag{8}$$

where OBG is the overburden stress gradient; P_p is the pore pressure gradient; and k_0 is the matrix stress or effective stress coefficient.

Eaton's method

Eaton (1969) used Poisson's ratio of the formation to calculate the fracture gradient based on the concept of the minimum injection pressure proposed by Hubbert and Willis (1957):

$$\nu = \frac{V_P^2 - 2V_S^2}{2(V_P^2 - V_S^2)} \tag{9}$$

$$P_{Fraction} = (P_{Overburden} - P_{Pore}) * \left(\frac{\nu}{1 - \nu}\right) + P_{pore} \tag{10}$$

where ν is Poisson's ratio, which can be obtained from the compressional and shear velocities (Vp and Vs) by Eq. (9) as a cube that is in the acceptable ranges between 0.2 and 0.1. Finally, using Eaton's Equation (1969), the formation fracture pressure is calculated according to Eq. (10).

Eaton's method enables the consideration of the effect of different rocks (e.g., shale, sandstone) on fracture gradient, because the lithology effect is considered in Poisson's ratio. In fact, Eq. (10) is the equation of the minimum value of the minimum stress derived from a uniaxial strain condition (Zhang and Yin 2017; Zhang et al. 2017).

Daines' method

Daines (1982) superposed a horizontal tectonic stress σ_t onto Eaton's equation. Expressing in the stress form, he called it as "minimum pressure within the borehole to hold open and extend an existing fracture," which can be written in Eq. (11):

$$\sigma_f = \left(\beta + \frac{\nu}{1 - \nu}\right)(\sigma_V - p) + p. \tag{11}$$

where σ_f is the fracture pressure; σ_v is the vertical stress, p is the pore pressure, and β is a constant.

Table 7 Experimental variogram computation for final pore pressure cubes

Direction	Azimuth	Dip	Number of lags	Lag distance	Search radius	Band width	Tolerance angle	Lag tolerance	Thickness
Vertical	NA	90	8	25	200	50	45	50	0.001
Major	0	0	8	250	2000	200	45	50	0.001
Minor	270	0	8	250	2000	200	45	50	0.001

Table 8 Results of Gaussian variogram of the pore pressure cube obtained by combining SGS and co-kriging methods with acoustic impedance (AI), and FFBP-NN methods in the study field

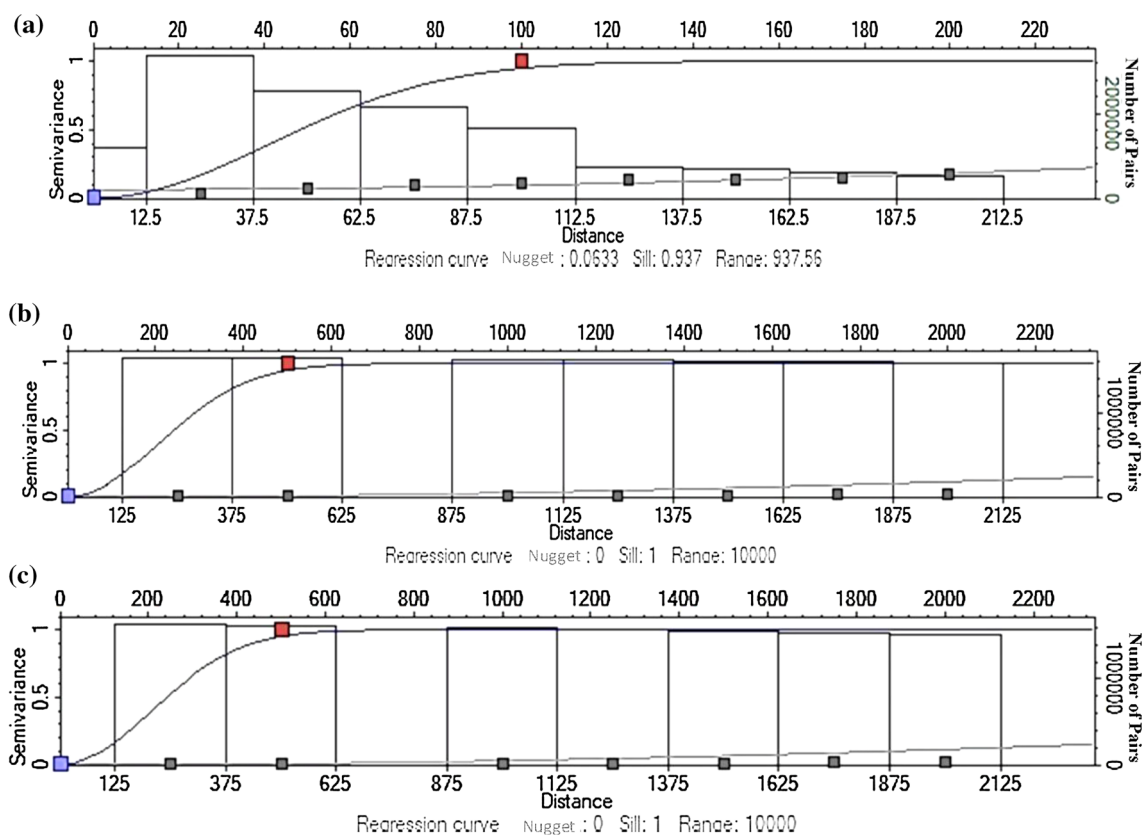| Direction	Nugget	Sill	Range	Number of pairs	Anisotropy range (m)
Vertical	0.0633	0.937	937.56	13,374,251	Vertical: 68
Major azimuth 0	0	1	10,000	11,367,363	Major direction:11,850
Minor azimuth 270	0	1	10,000	11,058,663	Minor direction:11,850

Fig. 10 Semi variogram of final Pore pressure Cube **a** vertical, **b** horizontal major direction azimuth zero deg., **c** minor direction azimuth 270 deg

Safe mud weight limits concept

Shear failure usually results in borehole collapse or breakout. Borehole breakouts are collapsed regions located on the least horizontal principal stress for vertical wells and are generally formed by compressive shear failure. Therefore, compressional failure will occur in the direction of the minimum horizontal stress because the tangential stress will reach a maximum here known as the lower limit of mud weight. In general, the borehole tensile failure is defined by the minimum principal stress (Darvishpour et al. 2019; Hoseinpour and Riahi 2022; Li et al. 2022; Li and Wu 2022). Therefore, this failure becomes the upper limit of the mud weight window in safe drilling operation (Anari and Ebrahimabadi 2018; Aslannezhad et al. 2016). In Fig. 4, the concept of safe mud weight window (SMMW) is depicted. As is seen from this figure, a low MW of below the pore pressure gradient will result in a kick. If the MW is less than the breakouts, pressure gradient shear failure will occur and the rocks fall into the wellbore. On the other side, increasing the MW above the magnitude of minimum stress will lead into invasion of the mud into the formation, i.e., mud loss.

Increasing the MW further above the fracture pressure gradient causes an induced fracture to be initiated in the wellbore wall (Le and Rasouli 2012; Nazarisaram and Ebrahimabadi 2022). In this study, the aim is to determine the two mud window limits of breakouts and breakdown or fracturing gradients for exploratory wellbores, but due to don't have geomechanical data resulting from drilling cores and leak-off test (LOT), fracture pressure calculated only by the Eaton method and SMMW determined by the equivalent method using pore and fracture pressures modeling resulting seismic interpretation and well logging data.

Results and discussion

Calculating the upper and lower limits of the drilling mud window requires drilling core data and conducting laboratory studies to calculate the minimum and maximum horizontal stress as well as vertical stress to conduct geomechanical and well stability studies. The drilled core from the exploratory wells of studied Azadegan Field only included four wells A-001 to A-004 in reservoir formations in limited depths. The above-mentioned cores were sent to the

Japanese TRC laboratory (2002) to calculate the shear velocity (Vs), and no other data is available. Therefore, it was not possible to calculate the parameters of shear failure and tensile failure, and an equivalent safe mud window to drilling mud using pore pressure with a confidence interval greater than + 50 PSI and fracture pressure with a confidence interval of less than − 50 PSI were used. Therefore, the proposal of this study conducts core drilling in new exploitation wells for the exact window of drilling mud using the calculation of breakout and breakdown pressures. Also, failure to conduct the leak-off test (LOT) at the beginning of drilling new hole sections in exploratory wells of the Azadegan Field due to the fear of formation failure was another challenge for calculating and calibrating the formation fracture pressure.

As the results, the maximum modeled MW is 150PCF in the upper Fahliyan Formation and mud heavier than 130 PCF starts from the Khalij member of the Gadvan Formation and continues to the bottom of the field. Comparing the drilled MW to the modeled MW changes shows a high correlation with the presented model results, especially in the Fahliyan reservoir Formation, where the MW has increased to more than 100 PCF, and the Ilam Formation, which has MW between 80 and 100 PCF. Finally, all of the mentioned methods are used to determine a synthetic well log which includes safe drilling mud weight. The results show that in the deep and ultra-deep reservoir formations, the calculated Safe MW is in good match with real data.

Considering the methodology described in Materials and Methods, by converting the above relation to exponential, the equation becomes $RHOB = 10^{(-0.427706)} V_p^{0.229185}$, so the Gardner relation coefficients are calculated as $a = 0.38$ and $b = 0.23$. Therefore, to calculate the average density using the average velocity cube, the check shot data and vertical seismic profiling (VSP) have been used to produce average velocity cube.

According to the results, the most changes in overburden pressure are 10,000–16,000 PSI.

Pore and fracture pressure variations

Based on comparing histograms of pressure changes, due to the small changes between the minimum and maximum values of pore pressure and fracture pressure in formations such as Kazhdumi and Gadvan at a rate of less than 200 PSI, to design a drilling mud window, safe interval values to prevent well flow and formation loss of about 50 PSI have been suggested. Based on the obtained results, the increase in pore and fracture pressures of the formation is quite noticeable with increasing depth, except for the lower Fahliyan Formation, in which, with an increasing depth, we see a pressure decrease in this formation. The maximum pore pressure of 10,000 PSI in the Gadvan Formation to the upper Fahliyan and the

Table 9 Changes in pore and fracture pressures based on modeling of formation pressures of South Azadegan Field

Formation	Pore pressure (psi)	Fracture pressure (psi)
Aghajari	76.2–87.2	94–142
Gachsaran	10–440	80–640
Asmari	100–3900	100–4900
Gurpi	2250–4700	2500–4900
Tarbur (Member)	3550–4900	3825–5125
Ilam and Laffan	4240–6160	4500–7550
Sarvak	4300–6550	4750–7550
Kazhdumi	4800–7100	5000–8200
Dariyan	5025–6425	5780–6680
Gadvan	4900–9900	5200–12,600
Khalij (member)	4800–10,000	5000–12,600
Upper Fahliyan	3500–10,000	4200–10,000
Lower Fahliyan to Gotnia	5000–9700	5400–13,000

maximum fracture pressure of 13,000 PSI in the Lower Fahliyan Formation to Gotnia have been obtained (Table 9).

Abnormal pore pressure gradient model

According to results, the studied field generally has an abnormal pore pressure gradient from the depth of 2000 m down in the range between 0.465 and 1 PSI/ft. (Fig. 11).

Designing the mud window range of drilling fluid

Calculating the minimum and maximum mud weight in the studied field

As mentioned, due to the impossibility of using breakout and breakdown pressure to calculate the upper and lower limits of the mud window, it is decided to employ pore and fracture pressure cubes with the highest possible precision. In consonance with the hydrostatic pressure concept, the lower and upper margins of the mud window will be calculated as Eqs. (12) and (13), respectively (Appendixes (18) to (20)).

It is required to explain that during several trial and error calculations, the most suitable safety margin in these cases should be regarded as ± 50 PSI. This pressure interval coincides with and confirms the losses and flows mentioned in daily drilling reports (DDR) of the Southern Azadegan Field, particularly Kazhdmi and Gadvan Formations. Notably, 0.5 PCF shifts in mud weight led to frequent losses and flows and, in some circumstances, an underground blowout in these formations. So, an equivalent safe mud window using pore pressure plus 50 PSI and fracture pressure minus 50 PSI was used as the confidence interval.
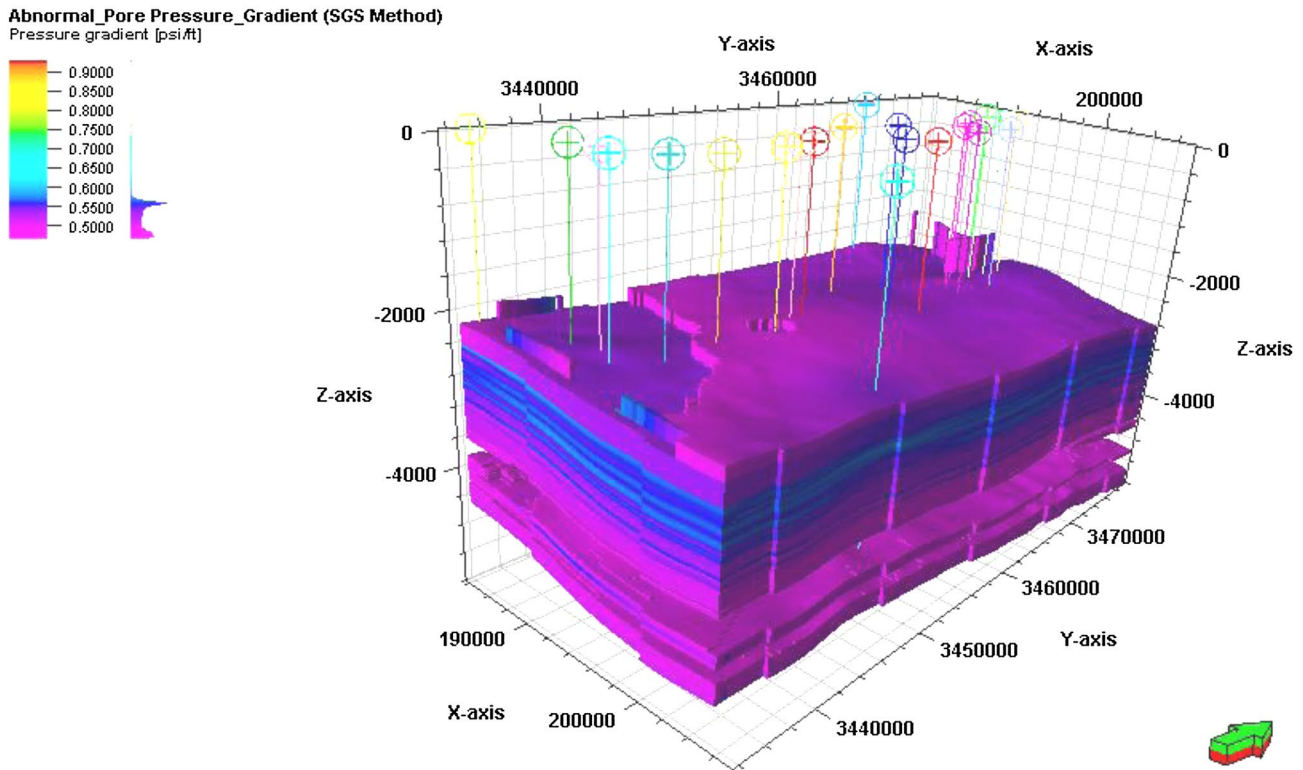
Fig. 11 Area with higher than normal pore pressure by SGS method in the studied field

By the pore pressure with a confidence interval greater than + 50 PSI and the depth in meters, the minimum mud weight (MW_{min}) in pounds per cubic foot (PCF) was calculated according to Eq. (12).

$$MW_{min} = \frac{(P_{pore} + 50psi) \times 144}{Depth \times 3.281} \tag{12}$$

Considering that the minimum MW for drilling with water is 62.4 PCF, values lower than this are removed from the initial cube. To complete the minimum MW cube, the SGS method was used along with co-kriging with the V_p cube. In the next step, to correct small out-of-range data, by checking the changes of the minimum MW histogram in different formations, the conditional programming of Petrel software was used. The minimum MW has been modified based on the depth changes and the initial MW range for Gachsaran to Gotnia and Aghajari surface Formations.

The maximum MW was calculated by having the fracture pressure with a confidence interval of less than -50 PSI and the depth in meters according to Eq. (13).

$$MW_{max} = \frac{(P_{Fracture} - 50psi) \times 144}{Depth \times 3.281} \tag{13}$$

In order to construct the initial cube of maximum MW, values less than 62.4 PCF are removed from the initial cube. To complete and correct the cube of the maximum MW, the same procedure was used as the previous method. Therefore, using the SGS method and correcting the out-of-range values by 5 PCF more than the similar distances in the minimum MW cube, the maximum MW based on the fracture pressure cube resulting from Eaton's relation was calculated (Fig. 12a and b).

Calculating the window of minimum and maximum mud weight changes

In order to calculate the mud window, the difference between the final MW cubes has been calculated. Due to the difference of more than 60 PCF and negative values in some places, the conditional programming relationship is used in Petrel software to modify the values.

According to results, the range of difference MW is between 2.5 and 30 PCF (Fig. 12c) and the maximum modeled MW is 150 PCF in the upper Fahliyan Formation. The

Fig. 12 Final cubes of **a** minimum MW (PCF), **b** maximum MW (PCF), **c** difference MW (between 2.5 and 30 PCF) in the South Azadegan Field
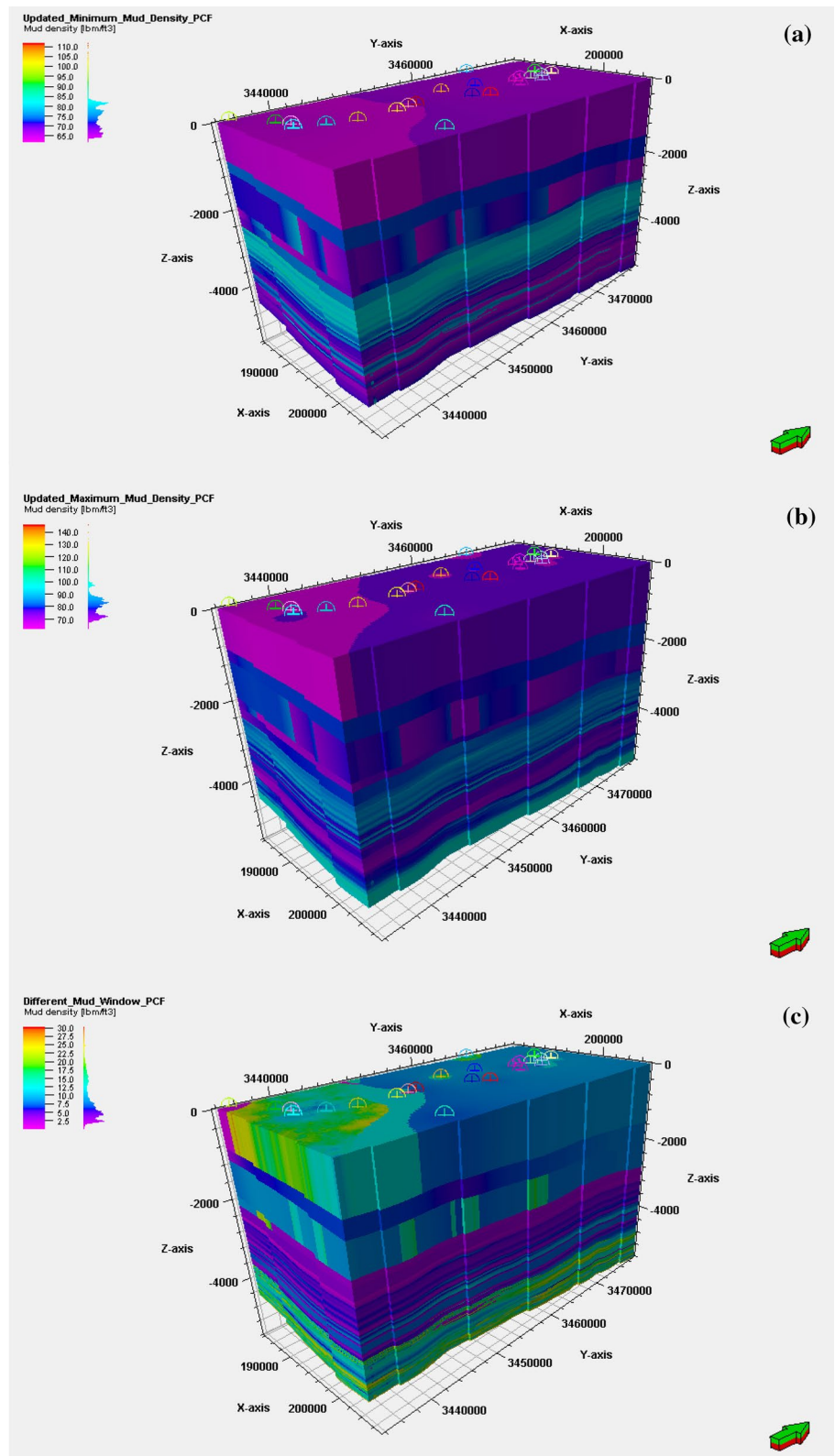
required interval for designing mud heavier than 130 PCF starts from the Khalij member and continues to the bottom of the field (Fig. 13 and Table 10).

The graphical results of mud weight cubes resulted by validating the minimum and maximum mud weight based
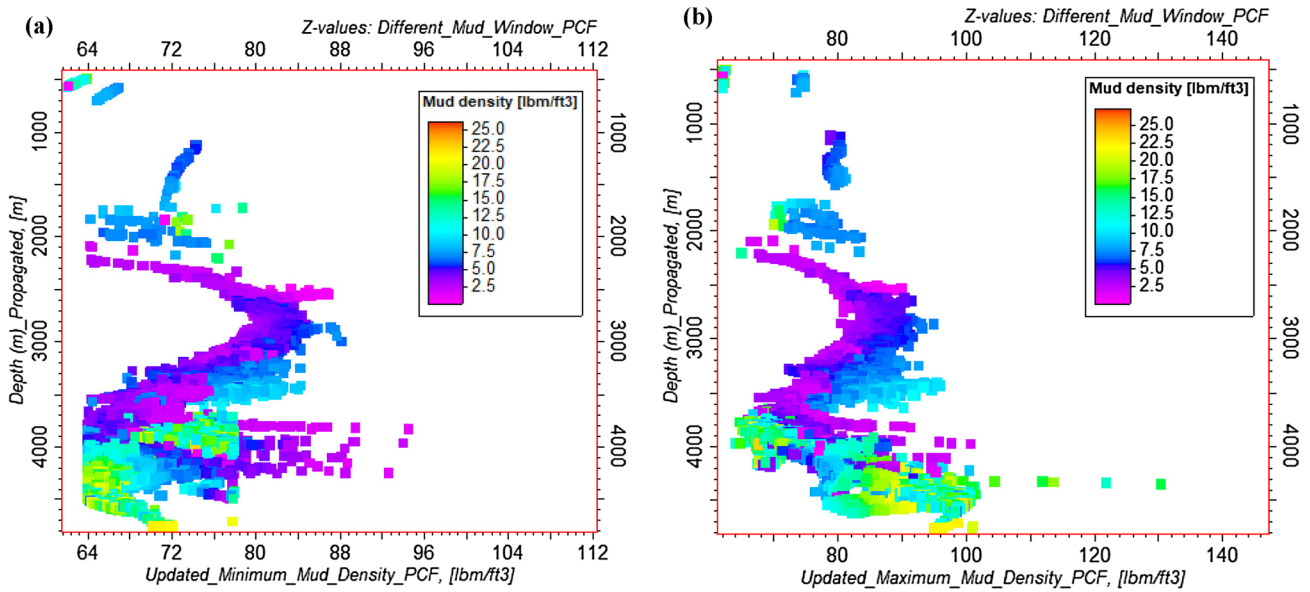
Fig. 13 Diagram of **a** minimum, **b** maximum values and changes in mud weight (PCF) based on increasing the depth of the studied field

Table 10 Variations in minimum and maximum mud weight (drilling mud window) based on pore and fracture pressures of the South Azadegan Formation

Formation	Min MW (PCF)	Max MW (PCF)	Different MW (PCF)
Aghajari (Surface)	62.5–67	62.5–75.6	0–7.5
Gachsaran	64.5–78.5	69.6–85.6	2–15.25
Asmari and Pabdeh	63.6–80.4	63.6–85.6	0–27
Gurpi	63.6–85.2	63.6–87	1–24.5
Tarbur (Member)	67.6–88.4	71.2–91.2	1.8–4.7
Ilam and Laffan	74.5–107	76–115	0–18.4
Sarvak	67–97.5	71–110	0–12.25
Kazhdumi	63.5–91.5	63.5–105	0–18.8
Dariyan	63.6–79.6	70.8–80.4	0.8–18
Gadvan	63–113	63–113	0–26.5
Khalij (member)	62.5–112	64–138	0–26
Upper Fahliyan	62.5–109	64–150	0–31
Lower Fahliyan to Gotnia	62–101	64–133	0–31

on the graphic well logs and removing out-of-range values are depicted in Figs. 12, 13,14.

Comparison of mud window model with the drilled exploratory wells

In order to validate the presented MW model, the graph of lithology, mud losses, and MW changes of some available exploratory wells has been used. A high correlation with the presented model results can be observed in comparing

the drilled MW changes to the modeled MW changes, especially in the Fahliyan reservoir Formation, where the MW has increased to more than 100 PCF, and the Ilam Formation, which has MW between 80–100 PCF (Fig. 14).

Synthetic logs of formation pressures and mud weight window

The final cubes were converted into equivalent synthetics logs for all 23 studied wells by Petrel software. In these synthetics logs, the window of changes in pore pressure and fracture pressure is on the left side (bold green and crimson diagrams). Also, the window of effective and overburden pressure changes in the middle (pink and dark blue diagrams) and the mud window diagram on the right side (blue and green diagrams) are presented. The main application of the above graphs is to examine the challenges ahead to overcome the formation pressures during drilling and to provide the appropriate MW to prevent the flow or loss of the exploitation wells in the vicinity of the above wells (Fig. 15).

Conclusions and Recomendation

To conclude all the results:

- Compressional velocity is successfully modeled using advanced geo-statistical approach (SGS combined with co-kriging) considering seismically inverted Acoustic Impedance as a trend to propagate sonic log through entire model boundary.
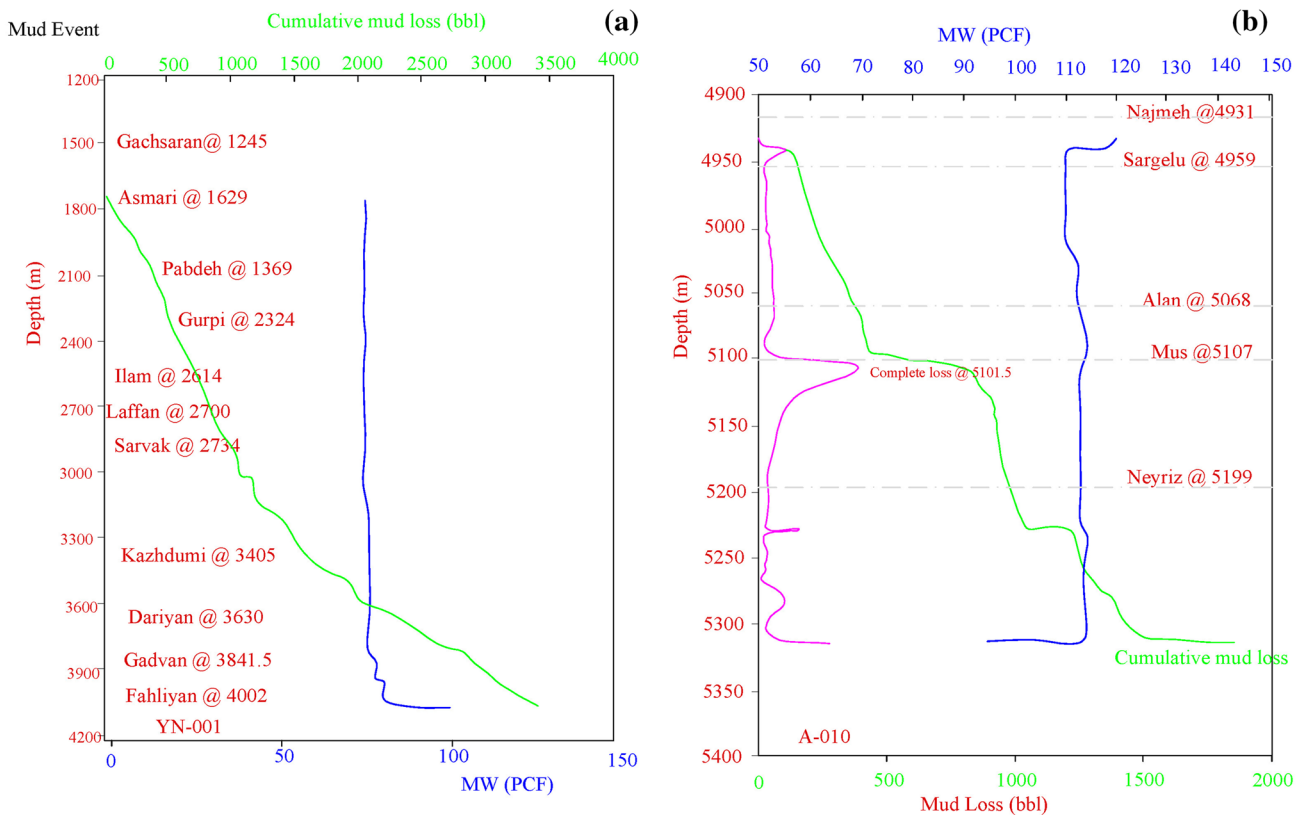
Fig. 14 Changes in mud weight (PCF) and accumulated mud loss of **a** YRN-001 exploratory well and **b** exploratory well of A-010 in the Jurassic deep formations below Gotnia (Mohammadi and Farhani 2010)

- Calculated pore pressure cube derived using statistical approaches (Bowers, SGS, and IDW) was validated by initial MDT data in 23 wells. Utilizing SGS for modeling pore pressure provides best fit (average 57%).
- Comparing velocity cubes and final effective pressure model (obtained through SGS) provides update in Bower's coefficients. So, the highest correlation coefficient between the final effective pressure cube and the velocity cube is related to the lower Fahliyan Formation with 0.86 and Ilam with 0.71.
- To design a drilling mud window, safe interval values to prevent well flow and formation loss of about 50 PSI have been suggested due to the small changes between the minimum and maximum values of pore pressure and fracture pressure in formations such as Kazhdumi and Gadvan in range of less than 200 PSI.
- Maximum pore and fracture pressures have been obtained in the Gadvan to the upper Fahliyan the Lower Fahliyan to Gotnia Formations, respectively. Also, the maximum modeled MW is 150PCF in the upper Fahliyan Formation.

- Utilizing conditional programming (*e.g., sequential and nested conditional expressions) to combine logs and cubes in a single model while removing out-of-range values* is a novel approach in this study.
- Comparing the drilled MW to the modeled MW changes shows a high correlation with the presented model results, especially in the Fahliyan reservoir Formation, where the MW has increased to more than 100 PCF, and the Ilam Formation, which has MW between 80 and 100 PCF.
- As an application of this study, equivalent synthetics formation pressures and mud window logs are presented to examine the challenges ahead to overcome the pressures of the formation during drilling and to provide the appropriate MW to prevent the flow or loss of the exploitation wells in the vicinity of the above wells.

It is suggested to use core laboratory test data in geomechanical studies of the South Azadegan Field to make better wellbore stability analysis. Also, analyzing it through the reservoir layers of the oil-bearing formations should
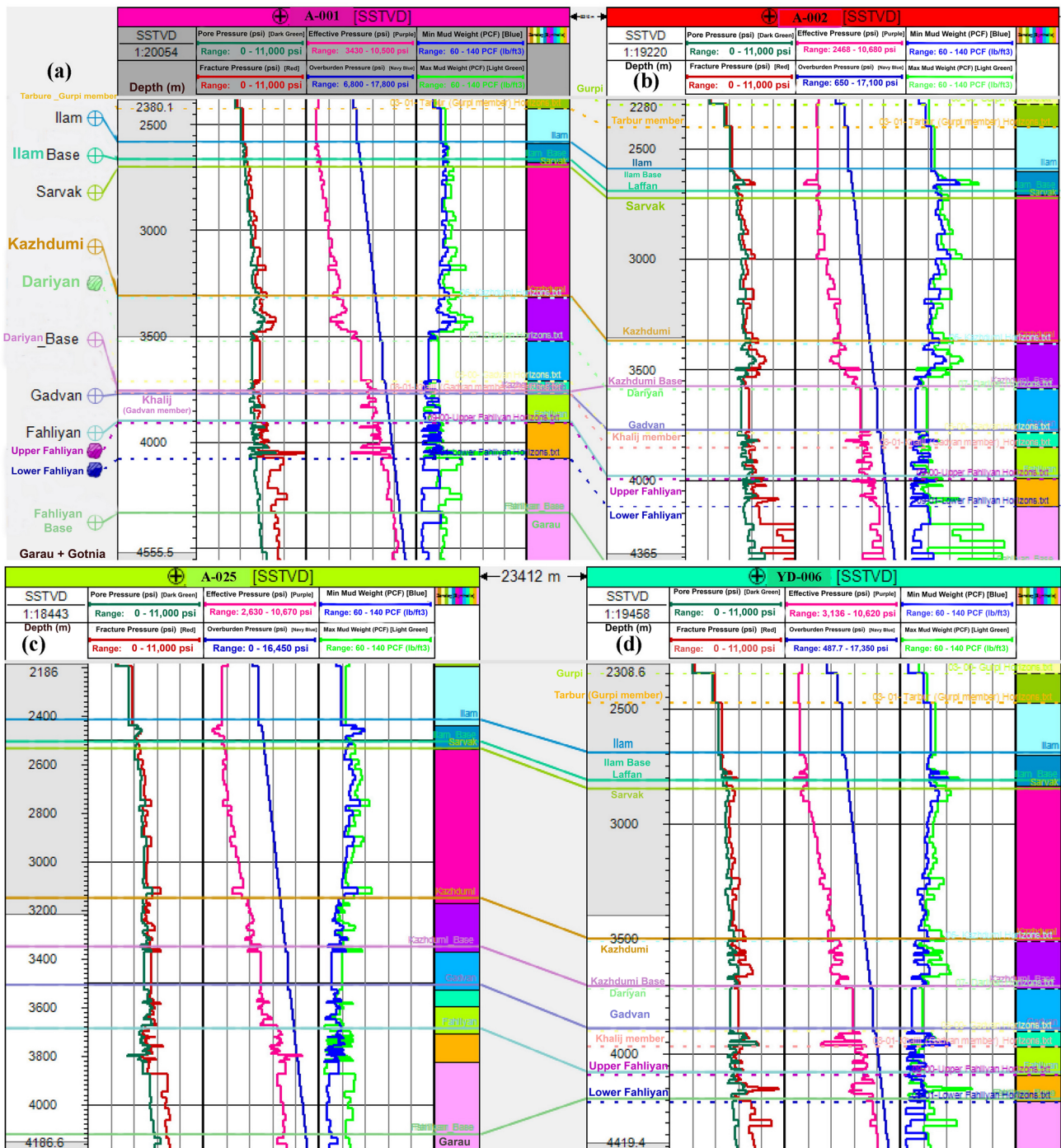
Fig. 15 Synthetic logs of changes in "pore pressure and fracture pressure," "effective pressure and overburden," and changes in "minimum and maximum mud weight" in **a** A-001, **b** A-002, **c** A-025, and **d** YD-006 exploratory wells

be investigated. The SMWW design and wellbore stability analysis could be done by FLAC3D software or other numerical simulators established with drilled strata geomechanical features. The initiation of plastic conditions could be used to determine SMWW in specific layers. Finally, the effects of rock strength parameters, major stresses around the wellbore, and pore pressure on the SMWW could be investigated for new wellbores.

Appendix 1

Appendix A: Conditional programming for determination of minimum & maximum mud weight cubes

See Fig. 16

Conditional programming with Petrel 2016 software to modify minimum mud weight cube (PCF), based on pore pressure cube (obtained from the neural network, sequential Gaussian simulation (SGS), and co-kriging method with Vp velocity model) for Gachsaran to Gotnia and also Aghajari surface Formations (Appendix Eqs. (14) and (15)).
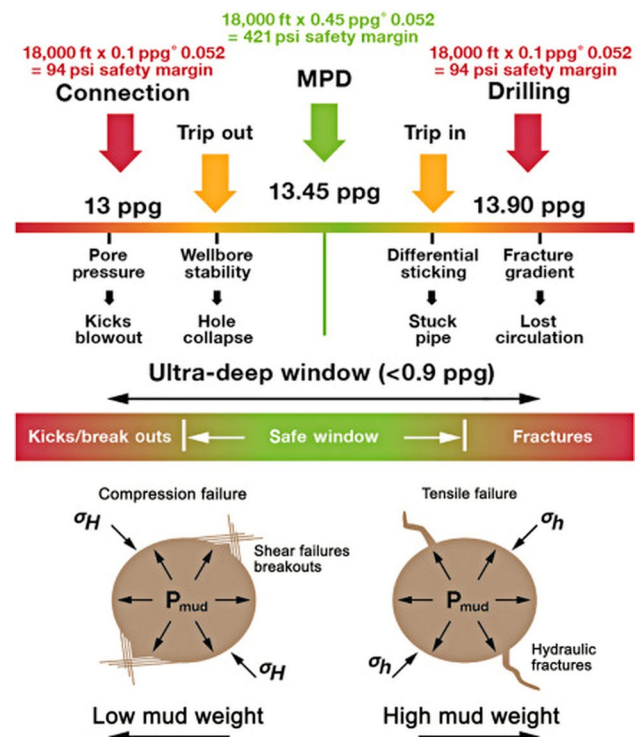
Fig. 16 Importance of mud weight management in narrow margin wells (William Abel 2019)

Updated_Maximum_Mud_Density_PCF = If(Maximum_Mud_Density_PCF >= 0 and Maximum_Mud_Density_PCF < 10 And Depth_m_Propagated > 1000,

Maximum_Mud_Density_PCF + 75, If(Maximum_Mud_Density_PCF >= 10 and Maximum_Mud_Density_PCF < 20 And Depth_m_Propagated > 1000,

Maximum_Mud_Density_PCF + 60, If(Maximum_Mud_Density_PCF >= 20 and Maximum_Mud_Density_PCF < 30 And Depth_m_Propagated > 1000,

Maximum_Mud_Density_PCF + 50, If(Maximum_Mud_Density_PCF >= 30 and Maximum_Mud_Density_PCF < 40 And Depth_m_Propagated > 1000,

Maximum_Mud_Density_PCF + 40, If(Maximum_Mud_Density_PCF >= 40 and Maximum_Mud_Density_PCF < 50 AndDepth_m_Propagated > 1000,

Maximum_Mud_Density_PCF + 30, If(Maximum_Mud_Density_PCF >= 50 and Maximum_Mud_Density_PCF < 64 And Depth_m_Propagated > 1000,

Maximum_Mud_Density_PCF + 20, If(Maximum_Mud_Density_PCF >= 5 And Maximum_Mud_Density_PCF < 10 And Depth_m_Propagated <= 1000,

Maximum_Mud_Density_PCF + 57, If(Maximum_Mud_Density_PCF >= 10 And Maximum_Mud_Density_PCF < 15 And Depth_m_Propagated <= 1000,

Maximum_Mud_Density_PCF + 60, If(Maximum_Mud_Density_PCF >= 15 And Maximum_Mud_Density_PCF < 20 And Depth_m_Propagated <= 1000,

Maximum_Mud_Density_PCF + 47, If(Maximum_Mud_Density_PCF > 0 And Maximum_Mud_Density_PCF < 5 And Depth_m_Propagated <= 1000,

Maximum_Mud_Density_PCF + 47, If(Maximum_Mud_Density_PCF > 0 And Maximum_Mud_Density_PCF < 5 And Depth_m_Propagated <= 1000,

Maximum_Mud_Density_PCF + 70, Maximum_Mud_Density_PCF)))))))))))

(14)

Conditional programming by Petrel 2016 software to modify the maximum mud weight cube (PCF) based on the fracture pressure cube of the formation (resulting from Eaton's relation) in Gachsaran to Gotnia and also Aghajari surface Formations.

Hydrostatic Pressure (HP)

$$= \frac{3.281 \times \text{Mud Weight} \times \text{True Vertical Depth (TVD)}}{144} \tag{19}$$

where Mud Weight in lb/ft (PCF), True Vertical Depth in meters.

Updated_Maximum_Mud_Density_PCF = If(Maximum_Mud_Density_PCF >= 0 and Maximum_Mud_Density_PCF < 10 And Depth_m_Propagated > 1000,

Maximum_Mud_Density_PCF + 75, If(Maximum_Mud_Density_PCF >= 10 and Maximum_Mud_Density_PCF < 20 And Depth_m_Propagated > 1000,

Maximum_Mud_Density_PCF + 60, If(Maximum_Mud_Density_PCF >= 20 and Maximum_Mud_Density_PCF < 30 And Depth_m_Propagated > 1000,

Maximum_Mud_Density_PCF + 50, If(Maximum_Mud_Density_PCF >= 30 and Maximum_Mud_Density_PCF < 40 And Depth_m_Propagated > 1000,

Maximum_Mud_Density_PCF + 40, If(Maximum_Mud_Density_PCF >= 40 and Maximum_Mud_Density_PCF < 50 And Depth_m_Propagated > 1000,

Maximum_Mud_Density_PCF + 30, If(Maximum_Mud_Density_PCF >= 50 and Maximum_Mud_Density_PCF < 64 And Depth_m_Propagated > 1000,

Maximum_Mud_Density_PCF + 20, If(Maximum_Mud_Density_PCF >= 5 And Maximum_Mud_Density_PCF < 10 And Depth_m_Propagated <= 1000,

Maximum_Mud_Density_PCF + 57, If(Maximum_Mud_Density_PCF >= 10 And Maximum_Mud_Density_PCF < 15 And Depth_m_Propagated <= 1000,

Maximum_Mud_Density_PCF + 60, If(Maximum_Mud_Density_PCF >= 15 And Maximum_Mud_Density_PCF < 20 And Depth_m_Propagated <= 1000,

Maximum_Mud_Density_PCF + 47, If(Maximum_Mud_Density_PCF > 0 And Maximum_Mud_Density_PCF < 5 And Depth_m_Propagated <= 1000,

Maximum_Mud_Density_PCF + 70, Maximum_Mud_Density_PCF))))))))))

$$\tag{15}$$

The difference of the MW cubes obtained by the SGS method is also calculated to achieve better results, which has fewer negative values than the original method. So to complete the MW difference cube, if there were empty parts (U) of the cube, the result of the SGS method was used according to the conditional programming Eqs. (16) and (17).

Different_Mud_Window_PCF =

    If((Updated_Maximum_Mud_Density_PCF − Updated_Minimum_Mud_Density_PCF) < 0 And

    (Updated_Maximum_Mud_Density_PCF − Updated_Minimum_Mud_Density_PCF) > 25, U,

    (Updated_Maximum_Mud_Density_PCF − Updated_Minimum_Mud_Density_PCF))

$$\tag{16}$$

Final_Different_Mud_Window_PCF =

    If(Different_Mud_Window_PCF = U,

    Different_Mud_Window_PCF_SGS,

    Different_Mud_Window_PCF)

$$\tag{17}$$

Hydrostatic pressure is defined as the pressure created by a fluid column, and two factors affecting hydrostatic pressure are mud weight and True Vertical Depth.

Calculate hydrostatic pressure in psi by using mud weight in pound per gallon (ppg) and feet as the units of True Vertical Depth. Hydrostatic pressure equation:

Hydrostatic Pressure (HP) = $0.052 \times$ Mud Weight

$$\times \text{ True Vertical Depth (TVD)} \tag{18}$$

where Mud Weight in ppg and True Vertical Depth in ft.

Also, Calculate hydrostatic pressure in psi by using mud weight in lb/ft3 and meter as the units of True Vertical Depth. Hydrostatic pressure equation:

So to estimate the minimum and maximum mud weight with formation pressures in hand and regarding safety margin (S.M), we can utilize the following equation:

$$MW_{\text{Min/max}} = \frac{(P_{\text{Pore/Fracture}} \pm S.M) \times 144}{\text{Depth} \times 3.281} \tag{20}$$

Mud weights and pressure management in complex wells, as illustrated in Appendix Fig. 16, command a greater understanding of the finer pressure measurement margin issues. It usually exists in low and high mud weight limits where lost time events can result if mud weight pressure aspects are not safely monitored and controlled (Bridges and Robinson 2020; William Abel 2019).
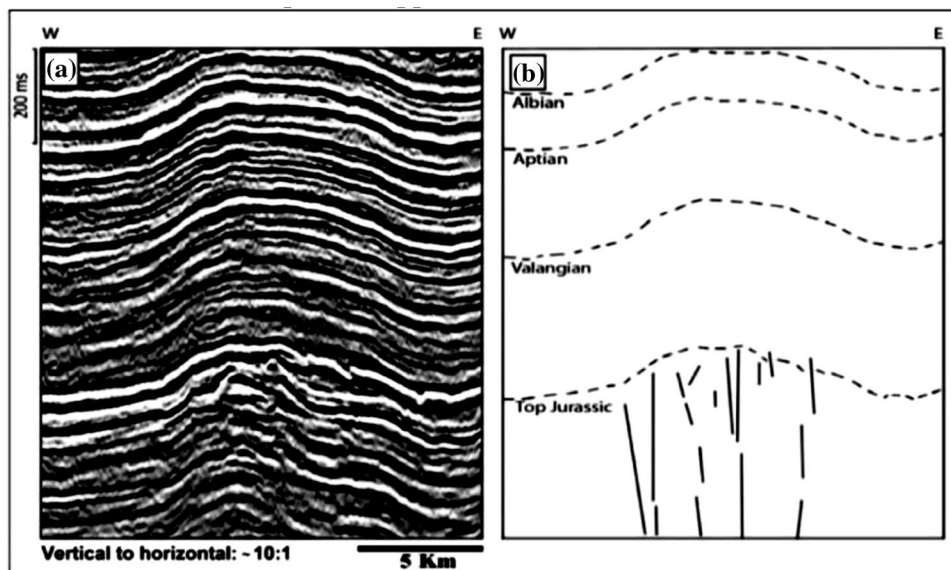
Appendix 2

Appendix B: Supplementary modeling steps

The Azadegan dome is a complex horst. Seismic data of the Azadegan structure show steep faulting in the core of the anticline. These faults die up in the upper Jurassic Gotnia Formation. Drill-hole and seismic data from the Azadegan anticline demonstrate unconformities and erosional surfaces due to the uplifting of basement-cored horsts.

Faults die up in the upper Jurassic gotnia formation

See Fig. 17

Fig. 17 Seismic profile across the Azadegan High, which shows a steep fault system in the Jurassic and underlying sedimentary rocks (Abdollahie Fard et al. 2006)
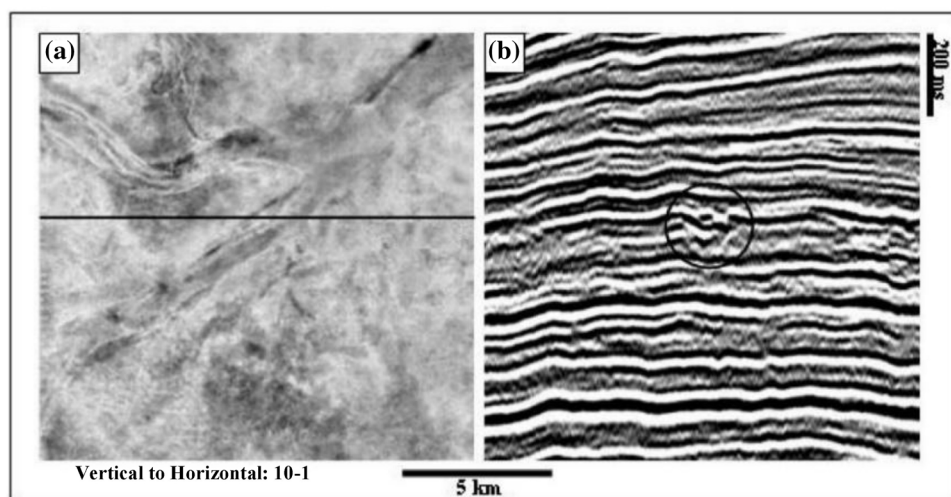

Appendix Fig. 17 shows incised channels in the top Cenomanian-Turonian Sarvak Formation indicate erosion of the anticline crest in the upper Cretaceous.

(a) indicates incised valleys filled by channel-type sediments. (b) shows the channel-type reflector pattern above the Turonian strata (Abdollahie Fard et al. 2006).

Geological modeling

See Fig. 18

After defining the network range, horizontal (I) and vertical (J) axes, number of nodes, and well's layout, the 3D geological structure of the field was modeled. Then, the In-line and X-line ranges of the amplitude values were added and a seismic cube with post-stack data was created by the arithmetic seismic resampling method of Petrel (2016) Software.

See Fig. 19

Fig. 18 **a** Root mean square volumetric seismic amplitude attribute map, within 30 ms of the upper Turonian sedimentary rocks. **b** Seismic profile through the Azadegan High (Abdollahie Fard et al. 2006)
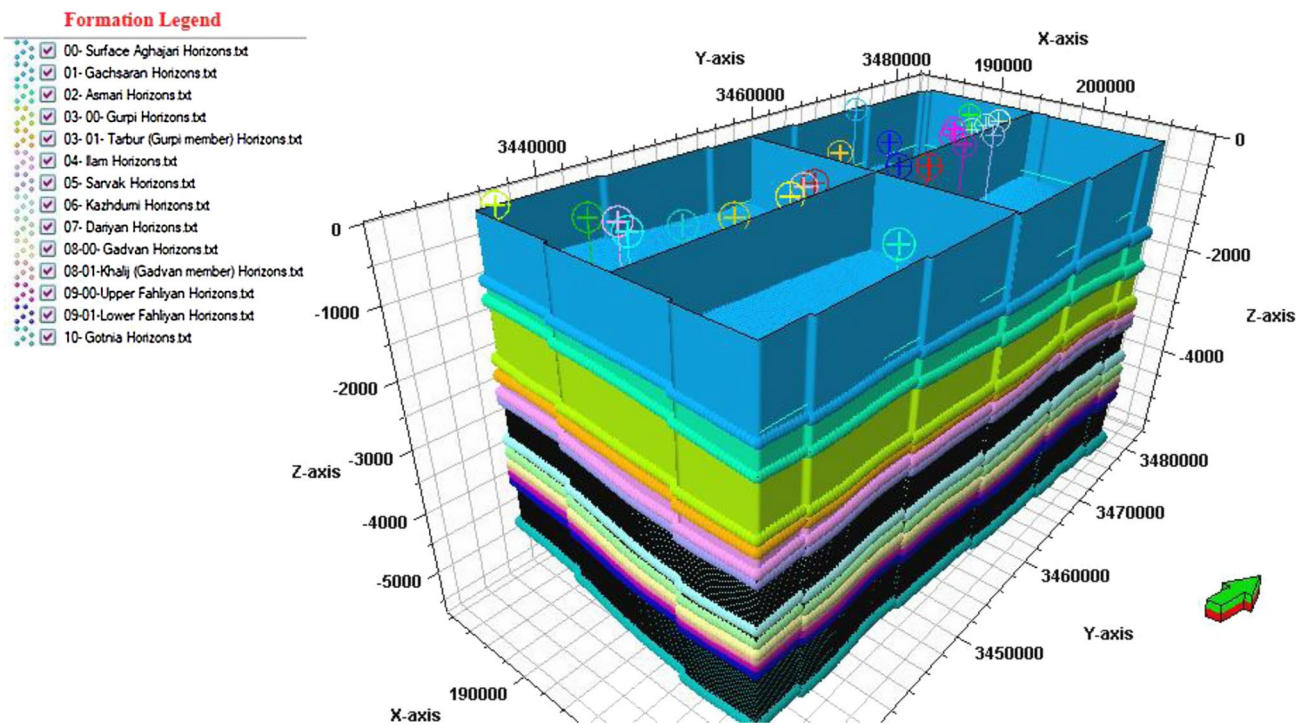
Fig. 19 Three-dimensional geological model of South Azadegan Field using seismic sections and drilling data along with the location of used wells

The initial cube of the minimum and maximum mud weight
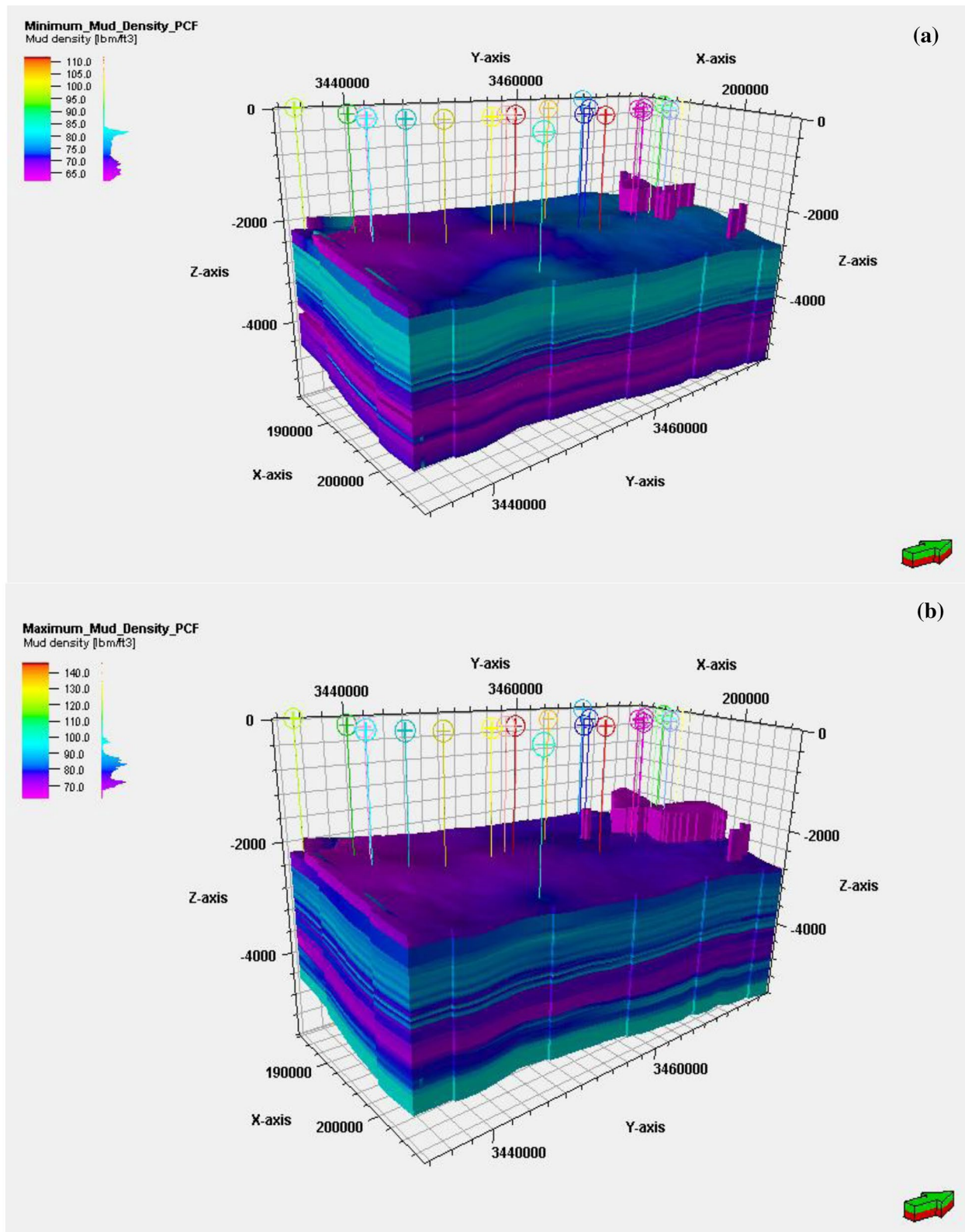
See Fig. 20

Fig. 20 Initial cube of **a** minimum mud weight based on pore pressure and adding 50 psi as a safety margin, considering the minimum weight of 62.4 PCF, **b** maximum mud weight based on the cube of the formation fracture pressure and deducting 50 PSI as a safety margin and considering the minimum weight of 62.4 PCF

General Histograms of mud weight changes in the studied field

See Fig. 21
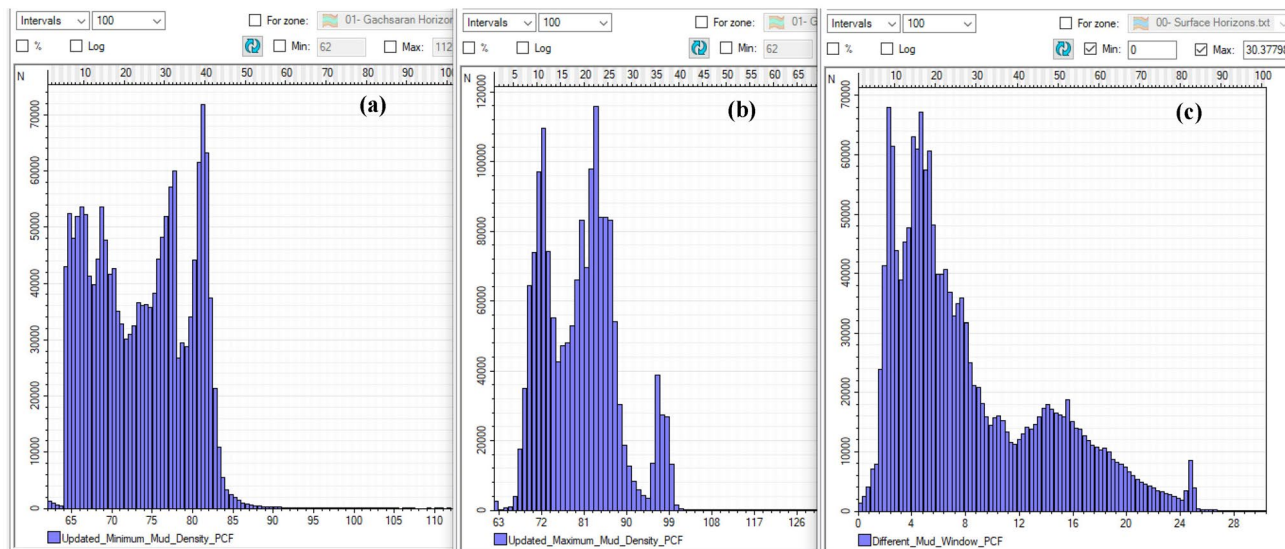
Fig. 21 General histogram of **a** minimum, **b** maximum, and **c** changes in mud weight based on the pressure model of the South Azadegan Field

Declarations

Conflict of interest The authors declare that they have no known competing financial interests or personal relationships that could have appeared to influence the work reported in this paper.

References

Aadnoy BS, Larsen K (1989) Method for fracture-gradient prediction for vertical and inclined boreholes. SPE Drill Eng 4(02):99–103. https://doi.org/10.2118/16695-pa

Abdelaal A, Elkatatny S, Abdulraheem A (2022) Real-time prediction of formation pressure gradient while drilling. Sci Rep 12(1):11318

Abdideh M, Fathabadi MR (2013) Analysis of stress field and determination of safe mud window in borehole drilling (case study: SW Iran). J Pet Explor Prod Technol 3(2):105–110

Abdollahie Fard I, Braathen A, Mokhtari M, Alavi A (2006) Structural models for the South Khuzestan area based on reflection seismic data. In: Shahid Beheshti University Tehran

Abdollahie Fard I, Hassanzadeh-Azar J (2002) Application of true dip and thichness attributes in seismic interpretation. J Earth Space Phys 28:17–23

Althaus VE (1975) A new model for fracture gradient. In: SPWLA 16th Annual Logging Symposium. OnePetro, New Orleans, Louisiana, pp SPWLA-1975-C

Anari R, Ebrahimabadi A (2018) An approach to select the optimum rock failure criterion for determining a safe mud window through wellbore stability analysis. Asian J Water Environ Pollut 15:127–140. https://doi.org/10.3233/AJW-180025

Anderson RA, Ingram DS, Zanier AM (1973) Determining fracture pressure gradients from well logs. J Petrol Technol 25(11):1259–1268. https://doi.org/10.2118/4135-pa

Andress J, Linn R (2016) Coding for penetration testers: building better tools. Syngress, pp 1–6. https://doi.org/10.1016/B1978-1010-1012-805472-805477.800018-805478

Armstrong M, Galli A, Beucher H, Loc'h G, Renard D, Doligez B, Eschard R, Geffroy F (2011) Plurigaussian simulations in geosciences. Springer Science Business Media

Aslannezhad M, Khaksar manshad A, Jalalifar H (2016) Determination of a safe mud window and analysis of wellbore stability to minimize drilling challenges and non-productive time. J Pet Explor Prod Technol 6(3):493–503

Baouche R, Sen S, Sadaoui M, Boutaleb K, Ganguli SS (2020) Characterization of pore pressure, fracture pressure, shear failure and

its implications for drilling, wellbore stability and completion design – A case study from the Takouazet field, Illizi Basin Algeria. Mar Pet Geol 120:104510

Baouche R, Sen S, Feriel HA, Radwan AE (2022) Estimation of horizontal stresses from wellbore failures in strike-slip tectonic regime: a case study from the ordovician reservoir of the Tinzaouatine Field, Illizi Basin Algeria. Interpretation 10(3):1–25

Beheshtian S, Rajabi M, Davoodi S, Wood DA, Ghorbani H, Mohamadian N, Alvar MA, Band SS (2022) Robust computational approach to determine the safe mud weight window using well-log data from a large gas reservoir. Mar Pet Geol 142:105772

Bohling G (2007) Introduction to Geostatistics in Hydro geophysics: theory, methods, and modeling. In: Boise State University, Boise, Idaho, p 50. http://people.ku.edu/~gbohling/BoiseGeostat

Bowers GL (1995) Pore pressure estimation from velocity data: Accounting for overpressure mechanisms besides undercompaction. SPE Drill Complet 10(02):89–95. https://doi.org/10.2118/27488-PA

Bowers GL (2002) Detecting high overpressure. Lead Edge 21(2):174–177

Breckels IM, van Eekelen HAM (1982) Relationship between horizontal stress and depth in sedimentary basins. J Petrol Technol 34(09):2191–2199. https://doi.org/10.2118/10336-pa

Bridges S, Robinson L (2020) Chapter 5 - Drilled solids calculations. In: Bridges S, Robinson L (eds) A Practical Handbook for Drilling Fluids Processing. Gulf Professional Publishing, pp 105–137

Constant WD, Bourgoyne AT Jr (1988) Fracture-gradient prediction for Offshore Wells. SPE Drill Eng 3(02):136–140. https://doi.org/10.2118/15105-pa

Daines SR (1982) Prediction of fracture pressures for wildcat wells. J Petrol Technol 34(04):863–872. https://doi.org/10.2118/9254-pa

Darvishpour A, Cheraghi Seifabad M, Wood DA, Ghorbani H (2019) Wellbore stability analysis to determine the safe mud weight window for sandstone layers. Pet Explor Dev 46(5):1031–1038

Du Y, Chen J, Cui Y, Xin J, Wang J, Li Y-Z, Fu X (2016) Genetic mechanism and development of the unsteady Sarvak play of the Azadegan oil field, southwest of Iran. Pet Sci 13(1):34–51. https://doi.org/10.1007/s12182-12016-10077-12186

Dutta NC, Bachrach R, Mukerji T (2021) Quantitative analysis of geopressure for geoscientists and engineers. Cambridge University Press, Cambridge, pp 501–531. https://doi.org/10.1017/9781108151726

Eaton BA (1969) Fracture gradient prediction and its application in oilfield operations. J Petrol Technol 21(10):1353–1360. https://doi.org/10.2118/2163-pa

Fredrich JT, Engler BP, Smith JA, Onyia EC, Tolman DN (2007) Predrill estimation of subsalt fracture gradient: analysis of the spa prospect to validate nonlinear finite element stress analyses. In: SPE/IADC Drilling Conference. https://doi.org/10.2118/105763-ms

Ganguli SS, Sen S (2020) Investigation of present-day in-situ stresses and pore pressure in the south Cambay Basin, western India: implications for drilling, reservoir development and fault reactivation. Mar Pet Geol 118:104422

Ganguli SS, Vedanti N, Akervoll I, Dimri VP (2016) Assessing the feasibility of CO2-enhanced oil recovery and storage in mature oil field: a case study from Cambay basin. J Geol Soc India 88(3):273–280

Ganguli SS, Vedanti N, Pandey OP, Dimri VP (2018) Deep thermal regime, temperature induced over-pressured zone and implications for hydrocarbon potential in the Ankleshwar oil field, Cambay basin, India. J Asian Earth Sci 161:93–102

Gardner GHF, Gardner LW, Gregory AR (1974) Formation velocity and density—the diagnostic basics for stratigraphic traPS. Geophysics 39(6):770–780

Gowida A, Ibrahim AF, Elkatatny S (2022) A hybrid data-driven solution to facilitate safe mud window prediction. Sci Rep 12(1):15773

Haimson B, Fairhurst C (1967) Initiation and extension of hydraulic fractures in rocks. Soc Petrol Eng J 7(03):310–318. https://doi.org/10.2118/1710-PA

Haris A, Sitorus R, Riyanto A (2017) Pore pressure prediction using probabilistic neural network: case study of South Sumatra Basin. In: IOP Conference Series: Earth and Environmental Science 62:012021

Hoseinpour M, Riahi MA (2022) Determination of the mud weight window, optimum drilling trajectory, and wellbore stability using geomechanical parameters in one of the Iranian hydrocarbon reservoirs. J Pet Explor Prod Technol 12(1):63–82. https://doi.org/10.1007/s13202-13021-01399-13205

Hosseini E, Gholami R, Hajivand F (2019) Geostatistical modeling and spatial distribution analysis of porosity and permeability in the Shurijeh-B reservoir of Khangiran gas field in Iran. J Pet Explor Prod Technol 9(2):1051–1073

Hu L, Deng J, Zhu H, Lin H, Chen Z, Deng F, Yan C (2013) A new pore pressure prediction method-back propagation artificial neural network. Electron J Geotech Eng 18:4093–4107

Hubbert MK, Willis DG (1957) Mechanics of hydraulic fracturing. Trans AIME 210(01):153–168

Jindal N, Biswal A (2016) Time-Depth modeling in high pore-pressure environment, Offshore East Coast of India.

Keaney G, Li G, Williams K (2010) Improved fracture gradient methodology-understanding the minimum stress In Gulf of Mexico. In: 44th U.S. Rock Mechanics Symposium and 5th U.S.-Canada Rock Mechanics Symposium

Kelkar M, Perez G (2002) Applied geostatistics for reservoir characterization. Soc Pet Eng. https://doi.org/10.2118/9781555630959

Khatibi S, Aghajanpour A (2020) Machine learning: a useful tool in geomechanical studies, a case study from an offshore gas field. Energies 13(14):3528. https://doi.org/10.3390/en13143528

Kianoush P, Mohammadi G, Hosseini SA, Keshavazr Faraj Khah N, Afzal P (2022) Compressional and shear interval velocity modeling to determine formation pressures in an oilfield of SW Iran. J Min Environ 13(3):851–873

Lantuéjoul C (2001) Geostatistical simulation: models and algorithms. Springer Science & Business Media, p 1139

Le K, Rasouli V (2012) Determination of safe mud weight windows for drilling deviated wellbores: a case study in the North Perth Basin. Petroleum 2012:83–95. https://doi.org/10.2495/PMR120081

Lee H, Jang Y, Kwon S, Park M-H, Mitra G (2018) The role of mechanical stratigraphy in the lateral variations of thrust development along the central Alberta Foothills Canada. Geosci Front 9(5):1451–1464

Li Q, Wu J (2022) Factors affecting the lower limit of the safe mud weight window for drilling operation in hydrate-bearing sediments in the Northern South China Sea. Geomech Geophys Geo-Energy Geo-Res 8(2):82. https://doi.org/10.1007/s11356-11021-18169-11359

Li Q, Wang F, Forson K, Zhang J, Zhang C, Chen J, Xu N, Wang Y (2022) Affecting analysis of the rheological characteristic and reservoir damage of CO2 fracturing fluid in low permeability shale reservoir. Environ Sci Pollut Res 29(25):37815–37826

Liguo Z, Zhu T, Hao T, Zhang X, Wang X, Zhang L (2020) Prediction method of formation pressure for the adjustment well in the reservoir with fault. J Phys: Conf Ser 1707:012012

Liu J, Chen P, Xu K, Yang H, Liu H, Liu Y (2022) Fracture stratigraphy and mechanical stratigraphy in sandstone: A multiscale quantitative analysis. Mar Pet Geol 145:105891

Matthews WR, Kelly J (1967) How to predict formation pressure and fracture gradient. Oil Gas J 65:1066–1092

Mehrkhani F, Ebrahimabadi A, Alaei MR (2019) Wellbore strengthening analysis in single and multi-fracture models using finite element and analytical methods, case study: South Pars Gas Field. In: 53rd U.S. Rock Mechanics/Geomechanics Symposium.

Mohammadi M, Farhani M (2010) Evaluation report of the Jurassic horizon of the well Azadegan-10. In: Exploration Directorate, General Directorate of Petroleum Engineering, Tehran, p 71

Morgan P (1999) Azadegan field geophysical interpretation. In: ConocoPhillips UK LTD, England

Nazarisaram M, Ebrahimabadi A (2022) Geomechanical design of Shadegan oilfield in order to modeling and designing ERD wells in Bangestan formations. J Pet Geomech 5(1):29–45. https://doi.org/10.22107/jpg.22022.349945.341173

Oriji AB, Ogbonna J (2012) A new fracture gradient prediction technique that shows good results in Gulf of Guinea. In: Abu Dhabi International Petroleum Conference and Exhibition. https://doi.org/10.2118/161209-ms

Pilkington PE (1978) Fracture gradient estimates in Tertiary basins. Pet Eng Int 8(5):138–148

Radwan AE (2021) Modeling pore pressure and fracture pressure using integrated well logging, drilling based interpretations and reservoir data in the Giant El Morgan oil Field, Gulf of Suez. Egypt J Afr Earth Sci 178:104165

Radwan A, Abudeif A, Attia M, Elkhawaga MA, Abdelghany WK, Kasem AA (2020) Geopressure evaluation using integrated basin modelling, well-logging and reservoir data analysis in the northern part of the Badri oil field, Gulf of Suez. Egypt J Afr Earth Sci 162:103743

Radwan AE (2020) Wellbore stability analysis and pore pressure study in Badri field using limited data, Gulf of Suez, Egypt. AAPG/datapages search and discovery Article 20476

Saadatnia N, Sharghi Y, Moghadasi J, Ezati M (2022) Fracture stability analysis during injection in one of the NFRs (naturally fractured reservoir) of the SW Iranian giant oil field. Arab J Geosci 16(1):27. https://doi.org/10.1007/s12517-12022-11062-w

Sadiq T, Nashawi I (2000) Using Neural Networks for Prediction of Formation Fracture Gradient

Sen S, Ganguli SS (2019) Estimation of pore pressure and fracture gradient in volve field, Norwegian North Sea. In: SPE Oil and Gas India Conference and Exhibition. https://doi.org/10.2118/194578-ms

Terzaghi K, Peck RB, Mesri G (1996) Soil mechanics in engineering practice. John Wiley & Sons, New York

Vessey I, Weber R (1984) Conditional statements and program coding: an experimental evaluation. Int J Man Mach Stud 21(2):161–190

Wessling S, Pei J, Bartetzko A, Dahl T, Wendt BL, Marti SK, Stevens JC (2009) Calibrating fracture gradients - an example demonstrating possibilities and limitations. In: International Petroleum Technology Conference. https://doi.org/10.2523/iptc-13831-ms

William Abel L (2019) Foreword. In: Aird P (ed) Deepwater Drilling. Gulf Professional Publishing, pp 7–8. https://doi.org/10.1016/B1978-1010-1008-102282-102285.109997-X

Woo J, Choi J, Yoon SH, Rhee CW (2022) Verification and application of sequence stratigraphy to reservoir characterization of Horn River Basin. Canada Min 12(6):776

Yin H, Cui H, Gao J (2022) Research on pore pressure detection while drilling based on mechanical specific energy. Processes 10(8):1481

Zhang J (2011) Pore pressure prediction from well logs: Methods, modifications, and new approaches. Earth Sci Rev 108(1):50–63. https://doi.org/10.1016/j.earscirev.2011.1006.1001

Zhang J (2013) Borehole stability analysis accounting for anisotropies in drilling to weak bedding planes. Int J Rock Mech Min Sci 60:160–170

Zhang JJ (2019) Chapter 9 - Fracture gradient prediction and wellbore strengthening. In: Zhang JJ (ed) Applied Petroleum Geomechanics. Gulf Professional Publishing, pp 337–374

Zhang J, Yin S-X (2017) Fracture gradient prediction: an overview and an improved method. Pet Sci 14(4):720–730

Zhang M, Zhang Y, Yu G (2017) Applied geostatisitcs analysis for reservoir characterization based on the SGeMS (stanford geostatistical modeling software). Open J Yangtze Oil Gas 2(1):45–66. https://doi.org/10.4236/ojogas.2017.21004

Zhang Z, Sun B, Wang Z, Pan S, Lou W, Sun D (2022) Formation pressure inversion method based on multisource information. SPE J 27(02):1287–1303

Zoback MD, Barton CA, Brudy M, Castillo DA, Finkbeiner T, Grollimund BR, Moos DB, Peska P, Ward CD, Wiprut DJ (2003) Determination of stress orientation and magnitude in deep wells. Int J Rock Mech Min Sci 40(7):1049–1076